

Phononic frictional losses of a particle crossing a crystal: linear-response theory

Gabriele Riva,¹ Giacomo Piscia,¹ Nicolas Trojani,¹ Giuseppe E. Santoro,^{2,3,4} Erio Tosatti,^{2,3,4} and Nicola Manini¹

¹*Dipartimento di Fisica, Università degli Studi di Milano, Via Celoria 16, 20133 Milano, Italy*

²*International School for Advanced Studies, Via Bonomea 265, 34136 Trieste, Italy*

³*The Abdus Salam International Center for Theoretical Physics, Strada Costiera 11, 34151 Trieste, Italy*

⁴*CNR-IOM Democritos National Simulation Center, Via Bonomea 265, 34136 Trieste, Italy*

We address weak-coupling frictional sliding with phononic dissipation by means of analytic many-body techniques. Our model consists of a particle (the "slider") moving through a two- or three-dimensional crystal and interacting weakly with its atoms, and therefore exciting phonons. By means of linear-response theory we obtain explicit expressions for the friction force slowing down the slider as a function of its speed, and compare them to the friction obtained by simulations, demonstrating a remarkable accord.

Keywords: Friction, sliding friction, kinetic friction, linear-response theory

I. INTRODUCTION

Nanofriction investigates the complex processes of transformation of mechanical energy into thermal energy, through excitation of the vibrational degrees of freedom (phonons) of solids, as well as electronic ones, when available. Friction phenomena between dry bodies occur on multiple length and time scales, from the macroscopic scale to the atomic scale. Also, they span from weak to strong magnitudes, from gentle wearless sliding to heavy, wear-rich scratching/ploughing. The present paper addresses the quantitative theory of a special wear-free friction at the atomic scale, namely that of weak-coupling phononic dissipation for a point-like classical particle channeling through a bulk crystal.

As a preamble, it must be noted that dynamical friction is rarely accessible to linear-response (LR) theory, because the coupling between "slider" and "substrate" and its effects are mostly far from weak, and the response elicited far from linear. However, a weak coupling situation in which LR works is realized in *two* well-defined limits. One is the popular low velocity, high temperature limit of a nanoscale slider. In that limit the thermal random walk of an initially freely diffusing microscopic slider is weakly perturbed by an infinitesimal

driving force field. The forcing gives rise to a mean average drift velocity with a corresponding frictional dissipation, both infinitesimal, connected to the initial random walk parameters through Einstein's fluctuation-dissipation theorem.¹⁻³ The second limit, opposite to the first, is realized when the slider's own velocity, momentum, or mass are so large that the disturbance caused to its motion can be altogether neglected. Such is, for instance, the general framework assumed in the dielectric theory of energy losses by fast particles crossing matter, long established for electronic excitations.^{4,5}

The present theory addresses the same fast slider limit, addressing phonon losses instead of electronic ones. It extends to a fast particle crossing, nearly unscathed, a 2D or 3D crystal, the results obtained earlier for a simple 1-dimensional (1D) model.^{6,7} Friction is evaluated as the loss of energy per unit time of a channeling particle that interacts weakly, through conservative short-range forces, with a vibrating crystal. The sliding particle, which in the following we still refer to as the "slider", traverses the crystal, generates phonon excitations, which we describe at a quantum level. The end result is the following formula for the friction force as a function of the slider velocity v_{SL} and the slider-crystal-atom interaction potential V (or rather its Fourier transform $\tilde{V}(\mathbf{Q})$):

$$F(v_{\text{SL}}) = \frac{4\pi}{ma^3} \sum_{\mathbf{G}_{\perp}} e^{-i\mathbf{x}_0 \cdot \mathbf{G}_{\perp}} \int_{\Omega} \frac{d^3Q}{(2\pi)^3} Q_x \tilde{V}(|\mathbf{Q}|) \tilde{V}(|\mathbf{Q} + \mathbf{G}_{\perp}|) e^{-W(\mathbf{Q}) - W(\mathbf{Q} + \mathbf{G}_{\perp})} \times \sum_{\lambda} \mathbf{Q} \cdot \boldsymbol{\epsilon}_{\lambda}(\mathbf{Q}) (\mathbf{Q} + \mathbf{G}_{\perp}) \cdot \boldsymbol{\epsilon}_{\lambda}(\mathbf{Q}) \frac{\gamma}{2\pi} \frac{4Q_x v_{\text{SL}}}{[(Q_x v_{\text{SL}} - \omega_{\lambda}(\mathbf{Q}))^2 + (\frac{\gamma}{2})^2] [(Q_x v_{\text{SL}} + \omega_{\lambda}(\mathbf{Q}))^2 + (\frac{\gamma}{2})^2]}. \quad (1)$$

Here the integration over the wave vector \mathbf{Q} extends over the octant Ω with all positive components. $\omega_{\lambda}(\mathbf{Q})$ and $\boldsymbol{\epsilon}_{\lambda}(\mathbf{Q})$ are the crystal's phonon frequencies and polarization vectors, respectively. \mathbf{G}_{\perp} are the reciprocal-lattice vectors perpendicular to the direction $\hat{\mathbf{x}}$ of the

slider velocity; \mathbf{x}_0 is the slider's initial position; $W(\mathbf{Q})$ are Debye-Waller factors; and γ is a coefficient quantifying the (weak) dissipation leading to phonon decay in the crystal. The predictions of Eq. (1) are validated by striking quantitative agreement with direct energy-loss

simulations. In the frictional context, the two opposite limits of low and large slider velocity were demonstrated in a molecular-dynamics (MD) simulation of a similar system, a gold cluster sliding on a graphene substrate, where the fast slider limit was designated as “ballistic”.⁸

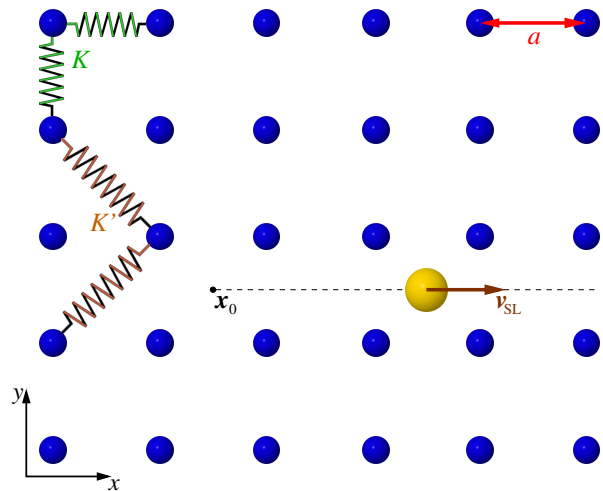
This paper is organized as follows. We introduce the model in Sect. II, detailing in particular the potential-energy function that describes the slider-crystal interaction. In Sect. III we report the theory leading to a general friction formula, Eq. (18), an expression relying on the density-density LR function χ_{nn}^R of the crystal. Section IV reports the derivation of Eq. (1), namely an explicit version of Eq. (18) based on the evaluation of χ_{nn}^R using a standard one-phonon approximation and on the assumption that the crystal comes with some intrinsic dissipation mechanism. In Sect. V we compare the analytic expression Eq. (1) with the friction evaluated numerically through molecular dynamics (MD) simulations. Section VI reports a version of the friction formula specialized to the 2D square-lattice crystal, also compared with 2D MD simulations. The present results and future extensions are discussed in Sect. VII.

II. THE MODEL

A sliding object, such as an AFM tip, gently grazing a flat crystal surface is slowed down by frictional phenomena. The kinetic energy of the slider decreases due to a sequence of collisions with the crystal, which generate excitations. In the present work, we omit the direct excitation of electrons and all kinds of triboelectric phenomena that can occur in real life. Focusing on insulators, within the adiabatic scheme, we address the excitation of phonons. These phonons, assumed to be harmonic, will ballistically propagate away, their energy and momentum lost by the slider. The realistic condition of a slider in contact with a surface involves necessarily all complications associated with the breaking of the lattice discrete invariance, resulting in surface phonons, e.g., Rayleigh waves. In the present paper we temporarily disregard surface effects, and consider the idealization of an infinitely extended perfect crystal, traversed by a slider that “channels” through it, as sketched in Fig. 1.

Our model harmonic crystal is characterized by particles of mass m that at equilibrium are arranged as a square (2D) or simple-cubic (3D) lattice. Harmonic nearest- and second-neighbor springs with elastic constants K and K' and equilibrium lengths a and $\sqrt{2}a$, respectively, guarantee the mechanical stability and determine the phonon dispersions.

In its simplest form, the slider is implemented as a point particle, characterized by mass M , position \mathbf{x}_{SL} and velocity \mathbf{v}_{SL} . More articulate structures of the slider are certainly possible, and were tested in the 1D context.⁶



The model can be formulated as follows:

$$H = H_{\text{harm}} + H_{\text{SL}} + \sum_j V(|\mathbf{x}_j - \mathbf{x}_{\text{SL}}(t)|), \quad (2)$$

where H_{harm} is the Hamiltonian for the harmonic lattice, $H_{\text{SL}} = \mathbf{p}_{\text{SL}}^2/(2M)$ is the Hamiltonian for the freely moving point slider, and the interaction couples the slider motion to all atoms in the harmonic crystal through a 2-body potential energy function $V(r)$. This model makes perfect sense for arbitrary kind and strength of this interaction potential, and for arbitrary channeling direction and velocity \mathbf{v}_{SL} . For general conditions, and whenever quantum-mechanical effects are negligible (such as could be approximately met in a real crystal at moderate temperature) it is relatively straightforward to investigate, e.g. by means of classical MD simulations involving a (sufficiently large) crystal portion. This model describes in microscopic detail the slider-crystal two-way energy and momentum transfer that, in time, leads to an overall slowing down of the slider and a progressive uptake of energy (heat) by the crystal. The instantaneous kinetic friction force experienced by the slider is quantified by its deceleration multiplied by the slider mass M . The same quantity averaged over a sufficiently long time allows us to estimate the mean kinetic friction

$$\mathbf{F}(t_1, t_2) = -M \frac{\mathbf{v}_{\text{SL}}(t_2) - \mathbf{v}_{\text{SL}}(t_1)}{t_2 - t_1} \quad (3)$$

that slows down the slider motion.

Aiming at an analytic evaluation of this mean kinetic friction, we introduce a few simplifying assumptions/approximations. The main assumption is that the interaction between the slider and the crystal is so weak

Physical quantity	natural units	typical values
length	a	500 pm
mass	m	5×10^{-26} kg
spring constant	K	300 N/m
time	$(m/K)^{1/2}$	1.3×10^{-14} s
frequency	$(K/m)^{1/2}$	7.7×10^{13} s
velocity	$a(K/m)^{1/2}$	3.9×10^4 m/s
force	Ka	1.5×10^{-7} N
energy	Ka^2	7.5×10^{-17} J
temperature	Ka^2/k_B	5.4×10^6 K
action	$a^2(Km)^{1/2}$	9.7×10^{-31} Js

TABLE I: Natural model units for the relevant physical quantities, with indications of plausible values relevant for a standard crystal. The natural energy scale represents the typical classical potential energy required to displace one atom away from its equilibrium position by one entire lattice spacing a , a quantity comparable to the crystal cohesive energy, and much larger than typical vibrational phonon quanta $\hbar\omega$.

that it perturbs the slider motion only over very long time scales. This allows us to adopt the first Born approximation of scattering theory: the slider moves at constant velocity

$$\mathbf{x}_{\text{SL}}(t) = \mathbf{x}_0 + \mathbf{v}_{\text{SL}}t, \quad (4)$$

as was done in the investigation of a similar 1D model.⁶ For the validity of this assumption, the kinetic energy of the particle, $\frac{1}{2}Mv_{\text{SL}}^2$, must be much larger than the typical energy transferred in the time taken by the slider to advance by one lattice spacing. This observation implies that, to be quantitatively valid, the adopted first Born approximation requires not only that the interaction strength is small, but also that the slider speed v_{SL} and mass M are sufficiently large.

We also assume that the slider moves along a crystal high-symmetry direction, say the x axis: $\mathbf{v}_{\text{SL}} = v_{\text{SL}}\mathbf{e}_x$. We also postulate that it starts off at a symmetric position \mathbf{x}_0 inside the crystalline “channel”, e.g. exactly midway between lines of atoms. In 2D, we take the symmetric slider’s initial position $\mathbf{x}_0 = \frac{a}{2}\mathbf{e}_y$, i.e. equidistant from the two adjacent atomic rows in the \mathbf{e}_x direction of the slider motion, see Fig. 1. In the 3D simple-cubic lattice, for \mathbf{x}_0 we test the following high-symmetry starting points in the $y-z$ plane: either at the centre of a square, $\mathbf{x}_0 = \frac{a}{2}(\mathbf{e}_y + \mathbf{e}_z)$, or at the midpoint of a bond, $\mathbf{x}_0 = \frac{a}{2}\mathbf{e}_y$. As we target a steady state, our analysis is independent of the component of the initial position in the sliding direction \mathbf{e}_x .

As was done for the 1D problem,⁶ it is convenient to express all mechanical quantities in natural units related to the crystal dynamics, listed in Table I. The main difference with the 1D model, where the unique speed of sound provides the natural unit of velocity, is that the 2D/3D crystals have multiple (transverse and longitudinal) speeds of sound, evaluated in Appendix A.

Nonetheless, all these speeds of sound are of the order of $a(K/m)^{1/2}$, which we adopt as the typical velocity unit, as indicated in Table I.

Within the discussed approximations, the slider dynamics becomes trivial, thus irrelevant. Accordingly, the Hamiltonian can be rewritten as that of a harmonic crystal weakly perturbed by the time-dependent interaction generated by the slider:

$$\begin{aligned} H &= H_{\text{harm}} + \sum_j V(|\mathbf{x}_j - \mathbf{x}_0 - \mathbf{v}_{\text{SL}}t|) \\ &= H_{\text{harm}} + \int d^3x V_{\text{ext}}(\mathbf{x}, t) n(\mathbf{x}). \end{aligned} \quad (5)$$

Here we have introduced the density operator

$$n(\mathbf{x}) = \sum_j \delta^{(3)}(\mathbf{x} - \mathbf{x}_j), \quad (6)$$

involving the position operator \mathbf{x}_j of the j -th atom, and the (weak) interaction potential energy $V_{\text{ext}}(\mathbf{x}, t) \equiv V(|\mathbf{x} - \mathbf{x}_0 - \mathbf{v}_{\text{SL}}t|)$ at a generic location \mathbf{x} in the crystal, as generated by the slider instantaneously visiting the location $\mathbf{x}_0 + \mathbf{v}_{\text{SL}}t$ at time t . This formulation is fully suitable for the application of the perturbative methods of quantum mechanics.

A. The interaction potential

The potential mediates the energy transfer to the harmonic crystal. It needs to be weak to make the perturbative approach meaningful. Note that, contrary to classical mechanics, in a quantum crystal the atomic positions are delocalized in space. The quantum probability distribution for \mathbf{x}_j spreads out across all space. As a consequence, the potential function $V(r)$ is evaluated at arbitrary values of its argument $r = |\mathbf{x} - \mathbf{x}_{\text{SL}}(t)|$. In particular, this separation r can take values arbitrarily close to zero, even if the slider remains “channeled” midway between atomic rows. For this reason, weak-coupling theory is incompatible with an interaction that diverges rapidly for $r \rightarrow 0$, such as e.g. a 6–12 Lennard-Jones (LJ) potential. Such kind of rapid divergence, would yield a diverging rate of collision between the slider and a crystal atom, regardless of how small the energy prefactor in V may be. Accordingly, our assumptions of weak interaction and constant velocity would be inappropriate for a sharply diverging potential function. A short-distance divergence $V \propto r^{-1}$ would be perfectly acceptable instead. Incidentally, note that the short-distance sharp divergence of the 6–12 LJ function is a realistic model for real-life atom-atom interactions down to small distances of the order of a fraction of the 1s shell radii, but below this distance any atom-atom interaction would transition to a $\propto r^{-1}$ milder divergence.

For the purpose of the present work, where we do not address any specific real-life condition, we decide to adopt

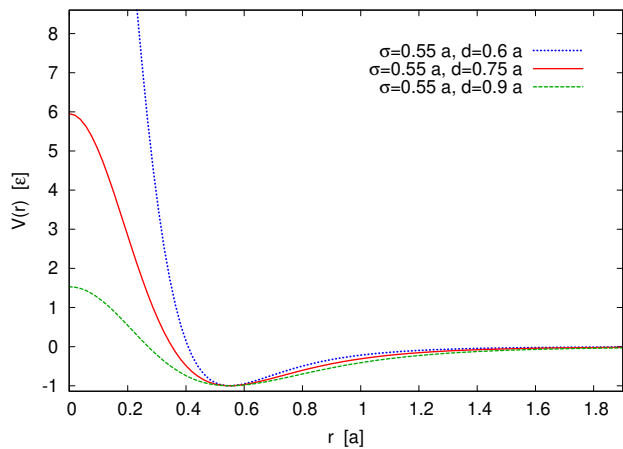


FIG. 2: The modified LJ function, Eq. (7), for $\sigma = 0.55a$ and a few values of the regularization length d . In the $d \rightarrow 0$ limit, the standard LJ potential is retrieved.

a potential that remains finite even at close distance. In practice we adopt a regularized LJ function, defined by:

$$V(r) = \varepsilon \left[\left(\frac{\sigma^2 + d^2}{r^2 + d^2} \right)^6 - 2 \left(\frac{\sigma^2 + d^2}{r^2 + d^2} \right)^3 \right]. \quad (7)$$

Figure 2 displays $V(r)$ for a few values of its parameters σ and d . This function has a minimum at distance $r = \sigma$ with depth $-\varepsilon$. d is a regularizing length, a parameter which makes $V(r)$ finite at any r . We adopt values of d of the same order as σ , so that the potential does not exceed a few times ε , even at small distance. The function in Eq. (7) is just a convenient example of model interaction potential: any sufficiently regular function that vanishes fast enough at large distance could be adopted in its place, e.g. a Yukawa potential, a Gaussian, a Woods-Saxon profile, etc.

According to Eq. (1), and in analogy to the 1D result of Ref. 6, this interaction $V(r)$ affects friction through its Fourier transform (FT), which needs to be carried out taking the dimensionality of the problem into account. Appendix E reports the calculation of the 3D FT of the function in Eq. (7):

$$\tilde{V}(q) = \varepsilon \frac{\pi^2(\sigma^2 + d^2)^3}{2d^3} e^{-qd} \left[\frac{(\sigma^2 + d^2)^3}{960d^6} (q^4 d^4 + 10q^3 d^3 + 45q^2 d^2 + 105qd + 105) - (qd + 1) \right]. \quad (8)$$

Figure 3a displays this FT for the same values of the parameters σ and d adopted for the real-space curves shown in Fig. 2.

Appendix F reports the derivation of the 2D FT, lead-

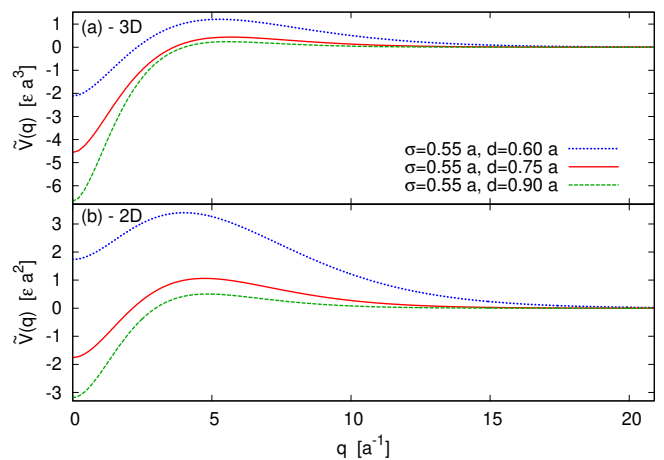


FIG. 3: The Fourier-transformed regularized LJ potential of Eq. (7), for the same values of σ and d as in Fig. 2. (a): 3D FT, Eq. (8); (b): 2D FT, Eq. (9). These functions enter the final expressions for friction, e.g. Eq. (1) as crucial ingredients.

ing to the following expression:

$$\tilde{V}(q) = 2\pi\varepsilon d^2 \left[\frac{1}{5!2^5} \left(1 + \frac{\sigma^2}{d^2} \right)^6 (qd)^5 K_5(qd) - \frac{1}{4} \left(1 + \frac{\sigma^2}{d^2} \right)^3 (qd)^2 K_2(qd) \right], \quad (9)$$

involving modified Bessel functions of the second kind $K_n(\cdot)$. Figure 3b illustrates the 2D FT of Eq. (9), for the same parameter values as in Fig. 2.

III. DISSIPATION AND FRICTION

We extend the LR approach carried out for the 1D model,^{6,7} to derive analytic expressions, the main example of which being Eq. (1), for the friction force experienced by the slider gently caressing a crystal. The weak-interaction regime is guaranteed by adopting a small interaction energy prefactor ε in Eq. (7).

The average friction force F can be evaluated by means of the dissipated power

$$\bar{W} = F v_{\text{SL}} \quad (10)$$

in the steady regime. The time average of the dissipated power must be executed over a period $\tau = a/v_{\text{SL}}$, namely over the time that it takes for the slider to advance across one lattice cell. To make this averaging possible, we assume that the slider advances along a crystal-commensurate direction, specifically (100): $\mathbf{v}_{\text{SL}} = v_{\text{SL}} \hat{\mathbf{x}}$. This assumption is fairly natural, since in practice channeling usually tends to self-align along crystal-commensurate directions.⁹ If instead the slider advanced in an arbitrary oblique direction (not identified by a set of integer Miller indexes), then the sliding process would not be periodic in time, and this would complicate the calculation of this time average \bar{W} .

We start from the instantaneous power transferred by the slider to the crystal due to the excitation of lattice vibrations. The straightforward generalization of the LR-theory expression Eq. (3) of Ref. 6 to a 3D geometry is

$$W = \frac{d}{dt}E(t) \simeq - \int d^3x \int d^3x' \int_{-\infty}^{\infty} dt' \quad (11)$$

$$V_{\text{ext}}(\mathbf{x}, t) \frac{\partial \chi_{nn}^R(\mathbf{x}, \mathbf{x}', t - t')}{\partial t} V_{\text{ext}}(\mathbf{x}', t').$$

$E(t)$ is the internal energy of the perturbed crystal at time t . Here $V_{\text{ext}}(\mathbf{x}, t)$ is the perturbation produced at time t by the slider following Eq. (4). As a result $V_{\text{ext}}(\mathbf{x}, t) = V(|\mathbf{x} - \mathbf{x}_0 - \mathbf{v}_{\text{SL}}t|)$. Also, $\chi_{nn}^R(\mathbf{x}, \mathbf{x}'; t - t') = -\frac{i}{\hbar}\theta(t - t')\langle[\hat{n}(\mathbf{x}, t), \hat{n}(\mathbf{x}', t')]\rangle$ is the retarded density-density response function of the unperturbed harmonic crystal.¹⁰ In 2D, the expression remains formally the same, except that the \mathbf{x} and \mathbf{x}' integrations are carried out over the appropriate 2D space.

We conveniently adopt a Fourier representation for the external potential:

$$V_{\text{ext}}(\mathbf{x}, t) = \int \frac{d^3q}{(2\pi)^3} e^{i\mathbf{q}\cdot(\mathbf{x}-\mathbf{x}_0-\mathbf{v}_{\text{SL}}t)} \tilde{V}(|\mathbf{q}|), \quad (12)$$

where the integration becomes $d^2q/(2\pi)^2$ in 2D. Taking advantage of the lattice translation invariance, we write the Fourier transform of the retarded response function as:

$$\chi_{nn}^R(\mathbf{x}, \mathbf{x}', t - t') = \sum_{\mathbf{G}} \int \frac{d^3Q}{(2\pi)^3} \int_{-\infty}^{+\infty} \frac{d\omega}{2\pi} e^{-i\omega(t-t')} \times$$

$$e^{i\mathbf{Q}\cdot\mathbf{x}} \chi_{nn}^R(\mathbf{Q}, \mathbf{Q} + \mathbf{G}, \omega) e^{-i(\mathbf{Q}+\mathbf{G})\cdot\mathbf{x}'}. \quad (13)$$

Here the \mathbf{G} vectors are the reciprocal lattice vector of the crystal. The sum over $\mathbf{G} = 2\pi a^{-1}(l_x, l_y, l_z)$ is understood as a sum over the (integer) Miller indexes l_x, l_y and l_z .

We now average the instantaneous power over one period, and reformulate Eq. (11) in the (\mathbf{Q}, ω) Fourier domain:

$$\bar{W} = \frac{1}{\tau} \int_0^\tau dt W(t) = -\frac{1}{\tau} \int_0^\tau dt \int d^3x \int d^3x' \int_{-\infty}^{\infty} dt' \times V_{\text{ext}}(\mathbf{x}, t) \frac{\partial \chi_{nn}^R(\mathbf{x}, \mathbf{x}', t - t')}{\partial t} V_{\text{ext}}(\mathbf{x}', t')$$

$$= -\frac{1}{\tau} \int_0^\tau dt \int d^3x \int d^3x' \int_{-\infty}^{\infty} dt' \int \frac{d^3q}{(2\pi)^3} \int \frac{d^3q'}{(2\pi)^3} \sum_{\mathbf{G}} \int \frac{d^3Q}{(2\pi)^3} \int_{-\infty}^{+\infty} \frac{d\omega}{2\pi} e^{-i\mathbf{q}\cdot\mathbf{x}_0} e^{i\mathbf{q}'\cdot\mathbf{x}_0} e^{i(\mathbf{q}+\mathbf{Q})\cdot\mathbf{x}} \times$$

$$e^{-i(\mathbf{q}'+\mathbf{Q}+\mathbf{G})\cdot\mathbf{x}'} e^{-it(\omega+\mathbf{q}\cdot\mathbf{v}_{\text{SL}})} e^{it'(\omega+\mathbf{q}'\cdot\mathbf{v}_{\text{SL}})} (-i\omega) \chi_{nn}^R(\mathbf{Q}, \mathbf{Q} + \mathbf{G}, \omega) \tilde{V}(|\mathbf{q}|) \tilde{V}(|\mathbf{q}'|).$$

The integrations over \mathbf{x}, \mathbf{x}' , and t' yield Dirac- δ functions over \mathbf{q}, \mathbf{q}' and ω , respectively. Accordingly:

$$\bar{W} = \frac{i}{\tau} \int_0^\tau dt \sum_{\mathbf{G}} e^{-i\mathbf{G}\cdot\mathbf{x}_0} e^{-it\mathbf{G}\cdot\mathbf{v}_{\text{SL}}} \int \frac{d^3Q}{(2\pi)^3} (\mathbf{Q} + \mathbf{G}) \cdot \mathbf{v}_{\text{SL}} \chi_{nn}^R(\mathbf{Q}, \mathbf{Q} + \mathbf{G}, (\mathbf{Q} + \mathbf{G}) \cdot \mathbf{v}_{\text{SL}}) \tilde{V}(|\mathbf{Q}|) \tilde{V}(|\mathbf{Q} + \mathbf{G}|)$$

$$= i \sum_{\mathbf{G}_\perp} e^{-i\mathbf{G}_\perp\cdot\mathbf{x}_0} \int \frac{d^3Q}{(2\pi)^3} \mathbf{Q} \cdot \mathbf{v}_{\text{SL}} \chi_{nn}^R(\mathbf{Q}, \mathbf{Q} + \mathbf{G}_\perp, \mathbf{Q} \cdot \mathbf{v}_{\text{SL}}) \tilde{V}(|\mathbf{Q}|) \tilde{V}(|\mathbf{Q} + \mathbf{G}_\perp|), \quad (14)$$

where we used the fact that the t integration $\int_0^\tau dt e^{-it\mathbf{G}\cdot\mathbf{v}_{\text{SL}}}$ vanishes whenever $\mathbf{G} \cdot \mathbf{v}_{\text{SL}} \neq 0$, and that

$$\int_0^\tau dt e^{-it\mathbf{G}\cdot\mathbf{v}_{\text{SL}}} = \tau \delta_{G_\parallel, 0}, \quad (15)$$

G_\parallel being the component of \mathbf{G} parallel of the sliding velocity, here simply the x component of \mathbf{G} . This leads to restricting the \mathbf{G} summation to \mathbf{G}_\perp , the component of \mathbf{G} perpendicular to \mathbf{v}_{SL} , i.e. in the yz plane. In 2D, the integration becomes $d^2Q/(2\pi)^2$, and \mathbf{G}_\perp coincides with the sole G_y component. In the expression for \bar{W} , Eq. (14), the only factor which depends on the initial position is $e^{-i\mathbf{G}_\perp\cdot\mathbf{x}_0}$. Clearly, the parallel (x) component of the ini-

tial position is irrelevant, since it corresponds to a trivial shift in time t , and the dissipated power is averaged over t anyway. For the adopted symmetrically-located channeling trajectories (see Sect. II), this \mathbf{x}_0 -related phase factor acquires either of the following simple expressions:

$$e^{-i\mathbf{G}_\perp\cdot\mathbf{x}_0} = (-1)^{l_y+l_z} \quad \text{if } \mathbf{x}_0 = \frac{a}{2}(\mathbf{e}_y + \mathbf{e}_z) \quad (16)$$

$$e^{-i\mathbf{G}_\perp\cdot\mathbf{x}_0} = (-1)^{l_y} \quad \text{if } \mathbf{x}_0 = \frac{a}{2}\mathbf{e}_y. \quad (17)$$

Equation (16) is relevant in the 3D geometry only, while Eq. (17) holds in both 3D and 2D.

In Appendix B we analyze the parity of the integrand of Eq. (14), arriving at Eq. (B7). That result proves that

the real part of $\chi_{nn}^R(\mathbf{Q}, \mathbf{Q} + \mathbf{G}_\perp, \mathbf{Q} \cdot \mathbf{v}_{\text{SL}}) \tilde{V}(|\mathbf{Q} + \mathbf{G}_\perp|) + \chi_{nn}^R(\mathbf{Q}, \mathbf{Q} - \mathbf{G}_\perp, \mathbf{Q} \cdot \mathbf{v}_{\text{SL}}) \tilde{V}(|\mathbf{Q} - \mathbf{G}_\perp|)$ is even under the transformation $\mathbf{Q} \rightarrow -\mathbf{Q}$, while its imaginary part is odd.

The full integrand of Eq. (14) can then be written as the product of a \mathbf{Q} -odd factor, namely $\mathbf{Q} \cdot \mathbf{v}_{\text{SL}}$, times

the term whose symmetry properties have just been discussed. As the \mathbf{Q} integration is carried out over an even domain, only the imaginary part of the retarded LR function contributes. The dissipated power and therefore the friction force, see Eq. (10), can then be expressed as:

$$F(v_{\text{SL}}) = \frac{\bar{W}}{v_{\text{SL}}} = - \sum_{\mathbf{G}_\perp} e^{-i\mathbf{G}_\perp \cdot \mathbf{x}_0} \int \frac{d^3 Q}{(2\pi)^3} \mathbf{Q} \cdot \hat{\mathbf{v}}_{\text{SL}} \text{Im} \chi_{nn}^R(\mathbf{Q}, \mathbf{Q} + \mathbf{G}_\perp, \mathbf{Q} \cdot \mathbf{v}_{\text{SL}}) \tilde{V}(|\mathbf{Q}|) \tilde{V}(|\mathbf{Q} + \mathbf{G}_\perp|), \quad (18)$$

where $\hat{\mathbf{v}}_{\text{SL}} = \mathbf{v}_{\text{SL}}/|\mathbf{v}_{\text{SL}}|$ is the velocity unit vector.

As both \tilde{V} factors in Eq. (18) are proportional to the coupling strength ε , in the weak-coupling regime addressed here the friction force is evidently a second-order, i.e. $\propto \varepsilon^2$, effect.

In the 1D problem of Ref. 6 the determination of the imaginary part of the density-density response function relied on the dynamic structure factor, which however led to an imprecise expression.⁷ Therefore, here we stick to the imaginary part of this response function, which we evaluate for the 2D or 3D harmonic crystal in Appendix C.

IV. EXPLICIT EXPRESSION FOR FRICTION

Starting from Eq. (18), we come now to derive and discuss an analytical expression for the friction force, as-

suming first a conservative crystal, and then a dissipative one characterized by a finite phonon lifetime.

A. Conservative crystal

We adopt the one-phonon approximation to the density-density response function, Eq. (C26), compute it for $\omega = \mathbf{Q} \cdot \mathbf{v}_{\text{SL}}$, and substitute it into Eq. (18), obtaining:

$$F(v_{\text{SL}}) = \frac{\pi}{2ma^3} \sum_{\mathbf{G}_\perp} e^{-i\mathbf{x}_0 \cdot \mathbf{G}_\perp} \int \frac{d^3 Q}{(2\pi)^3} \mathbf{Q} \cdot \hat{\mathbf{v}}_{\text{SL}} \tilde{V}(|\mathbf{Q}|) \tilde{V}(|\mathbf{Q} + \mathbf{G}_\perp|) e^{-W(\mathbf{Q})} e^{-W(\mathbf{Q} + \mathbf{G}_\perp)} \times \sum_{\lambda} \frac{\mathbf{Q} \cdot \boldsymbol{\epsilon}_\lambda(\mathbf{Q}) (\mathbf{Q} + \mathbf{G}_\perp) \cdot \boldsymbol{\epsilon}_\lambda(\mathbf{Q})}{\omega_\lambda(\mathbf{Q})} \left[\delta(\mathbf{Q} \cdot \mathbf{v}_{\text{SL}} - \omega_\lambda(\mathbf{Q})) - \delta(\mathbf{Q} \cdot \mathbf{v}_{\text{SL}} + \omega_\lambda(\mathbf{Q})) \right], \quad (19)$$

where $e^{-W(\mathbf{Q})}$ and $e^{-W(\mathbf{Q} + \mathbf{G}_\perp)}$ are Debye-Waller factors, see Eq. (C11). This expression is directly suitable for the calculation of friction. However it is conveniently simplified by taking advantage of the symmetry of the polarization vectors of the phonons of the simple-cubic lattice, as discussed in Appendix A, and summarised by Eq. (A13). With this information we can determine the parity of the integrand of Eq. (19) against reflections of each Cartesian component of the vector \mathbf{Q} .

Consider first the \mathbf{Q} components perpendicular to the slider velocity: Q_y and Q_z . The reflections $Q_y \rightarrow -Q_y$ and $Q_z \rightarrow -Q_z$ are equivalent by symmetry, thus we discuss the first one only. The factors $\tilde{V}(|\mathbf{Q}|)$, $e^{-W(\mathbf{Q})}$ and $\omega_\lambda(\mathbf{Q})$ are certainly even under this reflection. The

remaining part of Eq. (19) is:

$$\mathcal{T} = \sum_{\mathbf{G}_\perp} e^{-i\mathbf{x}_0 \cdot \mathbf{G}_\perp} \int \frac{d^3 Q}{(2\pi)^3} \tilde{V}(|\mathbf{Q} + \mathbf{G}_\perp|) e^{-W(\mathbf{Q} + \mathbf{G}_\perp)} \times \sum_{\lambda} \mathbf{Q} \cdot \boldsymbol{\epsilon}_\lambda(\mathbf{Q}) (\mathbf{Q} + \mathbf{G}_\perp) \cdot \boldsymbol{\epsilon}_\lambda(\mathbf{Q}).$$

We divide the $\mathbf{G}_\perp = \frac{2\pi}{a}(0, l_y, l_z)$ vectors into 3 sets: \mathcal{G}_\perp^0 including the $l_y = 0$ terms, \mathcal{G}_\perp^+ including those with $l_y >$

0, and \mathcal{G}_\perp^- those with $l_y < 0$. Therefore:

$$\begin{aligned} \mathcal{T} = & \left[\sum_{\mathbf{G}_\perp \in \mathcal{G}_\perp^0} + \sum_{\mathbf{G}_\perp \in \mathcal{G}_\perp^+} + \sum_{\mathbf{G}_\perp \in \mathcal{G}_\perp^-} \right] e^{-i\mathbf{x}_0 \cdot \mathbf{G}_\perp} \times \\ & \int \frac{d^3 Q}{(2\pi)^3} \tilde{V}(|\mathbf{Q} + \mathbf{G}_\perp|) e^{-W(\mathbf{Q} + \mathbf{G}_\perp)} \\ & \sum_\lambda \mathbf{Q} \cdot \boldsymbol{\epsilon}_\lambda(\mathbf{Q}) (\mathbf{Q} + \mathbf{G}_\perp) \cdot \boldsymbol{\epsilon}_\lambda(\mathbf{Q}). \end{aligned} \quad (20)$$

The \mathcal{G}_\perp^0 terms are clearly even under the $Q_y \rightarrow -Q_y$ transformation. Thanks to the discussed symmetry properties of the polarization vectors $\boldsymbol{\epsilon}_\lambda(\mathbf{Q})$, when we change $Q_y \rightarrow -Q_y$ the \mathcal{G}_\perp^+ summation becomes equal to the \mathcal{G}_\perp^- sum and vice versa. We conclude that the sum of Eq. (20), and therefore Eq. (19) is even with respect to

reflections of \mathbf{Q} in the directions perpendicular to the slider velocity.

As for the dependence on the parallel component $Q_x \equiv \mathbf{Q} \cdot \hat{\mathbf{v}}_{\text{SL}}$, the \mathcal{T} factor is certainly even under $Q_x \rightarrow -Q_x$. In Eq. (19) Q_x affects the factor

$$Q_x [\delta(Q_x v_{\text{SL}} - \omega_\lambda(\mathbf{Q})) - \delta(Q_x v_{\text{SL}} + \omega_\lambda(\mathbf{Q}))], \quad (21)$$

as well. We see that this factor is also even under $Q_x \rightarrow -Q_x$.

Thanks to these symmetry considerations, it is possible to restrict the momentum-space integration to the sub-domain Ω defined by $(Q_x \geq 0, Q_y \geq 0, Q_z \geq 0)$, provided that a factor 8 is included to account for the omitted integration sectors. For positive v_{SL} , the anti-resonant condition $\delta(Q_x v_{\text{SL}} + \omega_\lambda(\mathbf{Q}))$ never occurs in the Ω sub-domain, which allows us to simplify Eq. (19) to:

$$\begin{aligned} F(v_{\text{SL}}) = & \frac{4\pi}{ma^3} \sum_{\mathbf{G}_\perp} e^{-i\mathbf{x}_0 \cdot \mathbf{G}_\perp} \int_\Omega \frac{d^3 Q}{(2\pi)^3} Q_x \tilde{V}(|\mathbf{Q}|) \tilde{V}(|\mathbf{Q} + \mathbf{G}_\perp|) e^{-W(\mathbf{Q}) - W(\mathbf{Q} + \mathbf{G}_\perp)} \times \\ & \sum_\lambda \frac{\mathbf{Q} \cdot \boldsymbol{\epsilon}_\lambda(\mathbf{Q}) (\mathbf{Q} + \mathbf{G}_\perp) \cdot \boldsymbol{\epsilon}_\lambda(\mathbf{Q})}{\omega_\lambda(\mathbf{Q})} \delta(Q_x v_{\text{SL}} - \omega_\lambda(\mathbf{Q})). \end{aligned} \quad (22)$$

This is one of the main analytic results of the present paper: an explicit expression for the friction force as a function of the slider velocity for a classical particle channelling at a constant velocity through a conservative simple-cubic harmonic crystal. For the 2D version of Eq. (22), we defer to Sect. VI. Equation (22) expresses the friction as a summation over the \mathbf{G} vectors perpendicular to the sliding direction of \mathbf{Q} -space integrals of products of (i) Fourier components of the slider-crystal interaction, (ii) Debye-Waller factors, (iii) projections of the phonon polarization vectors in the \mathbf{Q} and $\mathbf{Q} + \mathbf{G}$ directions, the ratio $Q_x/\omega_\lambda(\mathbf{Q})$, and (iv) a Dirac delta imposing the resonance condition

$$\omega_\lambda(\mathbf{Q}) = \mathbf{Q} \cdot \mathbf{v}_{\text{SL}}, \quad (23)$$

namely that the product $\mathbf{Q} \cdot \mathbf{v}_{\text{SL}} \equiv Q_x v_{\text{SL}}$ matches the

phonon frequency at the same \mathbf{Q} point.

This Dirac-delta allows us to restrict the \mathbf{Q} -integration using the following identity:

$$\int_\Omega d^3 Q g(\mathbf{Q}) \delta(f(\mathbf{Q})) = \int_{S^\Omega} d^2 Q \frac{g(\mathbf{Q})}{|\nabla f(\mathbf{Q})|}, \quad (24)$$

where S^Ω is the 2D manifold which solves the equation $f(\mathbf{Q}) = 0$ in the Ω subset of the \mathbf{Q} space. In our Eq. (22), $f(\mathbf{Q}) = \mathbf{Q} \cdot \mathbf{v}_{\text{SL}} - \omega_\lambda(\mathbf{Q})$. As a consequence, S^Ω is the manifold of solutions of Eq. (23) for phonon branch λ ; additionally, the gradient $\nabla f(\mathbf{Q}) = \mathbf{v}_{\text{SL}} - \mathbf{v}_\lambda(\mathbf{Q})$, where $\mathbf{v}_\lambda(\mathbf{Q}) \equiv \nabla_{\mathbf{Q}} \omega_\lambda(\mathbf{Q})$ is the group velocity associated to phonon branch λ . Accordingly, the implementation of the recipe (24) transforms Eq. (22) to

$$F(v_{\text{SL}}) = \frac{4\pi}{ma^3} \sum_{\mathbf{G}_\perp} e^{-i\mathbf{x}_0 \cdot \mathbf{G}_\perp} \sum_\lambda \int_{S^\Omega_\lambda} \frac{d^2 Q}{(2\pi)^3} Q_x \tilde{V}(|\mathbf{Q}|) \tilde{V}(|\mathbf{Q} + \mathbf{G}_\perp|) e^{-W(\mathbf{Q}) - W(\mathbf{Q} + \mathbf{G}_\perp)} \frac{\mathbf{Q} \cdot \boldsymbol{\epsilon}_\lambda(\mathbf{Q}) (\mathbf{Q} + \mathbf{G}_\perp) \cdot \boldsymbol{\epsilon}_\lambda(\mathbf{Q})}{\omega_\lambda(\mathbf{Q}) |\mathbf{v}_{\text{SL}} - \mathbf{v}_\lambda(\mathbf{Q})|}. \quad (25)$$

As we lack analytic formulas for the 3D dispersion relations $\omega_\lambda(\mathbf{Q})$, we cannot express the manifolds S^Ω explic-

itly, and therefore we do not see how to further simplify Eq. (25).

Nevertheless, this formulation is highly instructive and useful as it stands. Equation (25) indicates that (i) friction comes from the additive contribution of the three phonon branches; (ii) at any given velocity \mathbf{v}_{SL} , friction is determined uniquely by a well-defined set of phonon modes, namely those that lie on the S_λ^Ω surfaces in Q space; (iii) especially large friction is expected from the contribution to the integral of phonons satisfying the “shock-wave” condition

$$\mathbf{v}_{\text{SL}} = \mathbf{v}_\lambda(\mathbf{Q}), \quad (26)$$

that makes the denominator vanish. We shall return to this shock-wave condition below.

Note importantly that, regardless of the sliding speed v_{SL} , for each phonon branch λ , there certainly exists some nonempty S_λ^Ω surface. The reason is that the condition (23) for \mathbf{Q} sitting on the S_λ^Ω surface can certainly be met at least at sufficiently remote (i.e. large $|Q_x|$ or large

$|Q_{y/z}|$) regions of \mathbf{Q} space. As a result, for any speed v_{SL} the conservative crystal keeps resonant phonon dissipation channels open, resulting in nonzero friction. This finding is qualitatively different from what was found for the 1D model:⁶ in 1D, when v_{SL} exceeds the speed of sound, no energy transfer to the conservative chain is possible, leading instead to vanishing friction for supersonic sliding.

B. Dissipative crystal

We proceed now to verify how a weak decay of the phonons in the crystal affects friction. By substituting the one-phonon approximation of the density-density response function of the dissipative crystal, Eq. (C30), into Eq. (18) we obtain:

$$F(v_{\text{SL}}) = \frac{\pi}{2ma^3} \sum_{\mathbf{G}_\perp} e^{-i\mathbf{x}_0 \cdot \mathbf{G}_\perp} \int \frac{d^3Q}{(2\pi)^3} Q_x \tilde{V}(|\mathbf{Q}|) \tilde{V}(|\mathbf{Q} + \mathbf{G}_\perp|) e^{-W(\mathbf{Q}) - W(\mathbf{Q} + \mathbf{G}_\perp)} \times \sum_{\lambda} \mathbf{Q} \cdot \boldsymbol{\epsilon}_\lambda(\mathbf{Q}) (\mathbf{Q} + \mathbf{G}_\perp) \cdot \boldsymbol{\epsilon}_\lambda(\mathbf{Q}) \mathcal{L}(\mathbf{Q}, v_{\text{SL}}, \gamma), \quad (27)$$

with

$$\mathcal{L}(\mathbf{Q}, v_{\text{SL}}, \gamma) = [\omega_\lambda(\mathbf{Q})]^{-1} \left[\frac{\frac{\gamma}{2\pi}}{(Q_x v_{\text{SL}} - \omega_\lambda(\mathbf{Q}))^2 + (\frac{\gamma}{2})^2} - \frac{\frac{\gamma}{2\pi}}{(Q_x v_{\text{SL}} + \omega_\lambda(\mathbf{Q}))^2 + (\frac{\gamma}{2})^2} \right] \quad (28)$$

$$= \frac{\gamma}{2\pi} \frac{4Q_x v_{\text{SL}}}{[(Q_x v_{\text{SL}} - \omega_\lambda(\mathbf{Q}))^2 + (\frac{\gamma}{2})^2][(Q_x v_{\text{SL}} + \omega_\lambda(\mathbf{Q}))^2 + (\frac{\gamma}{2})^2]}. \quad (29)$$

The formulation (29) explicitly clarifies that no singularity arises at the \mathbf{Q} points where $\omega_\lambda(\mathbf{Q})$ vanishes, and was anticipated in Eq. (1) in the Introduction. Dimensionally, the quantity $\mathcal{L}(\mathbf{Q}, v_{\text{SL}}, \gamma)$ is a squared time and combines the double Lorentzian terms with the inverse phonon-frequency dependence in the response function of Eq. (C30). The integrand function in Eq. (27) exhibits the same symmetries against reflections in the Q_y and Q_z components perpendicular to v_{SL} , as discussed above for the conservative crystal. As for the $Q_x \rightarrow -Q_x$ reflection, all factors are symmetric, except for Q_x in the first line and the function $\mathcal{L}(\mathbf{Q}, v_{\text{SL}}, \gamma)$: both these terms change sign under this reflection. As a result, the integrand function is fully symmetric against all $Q_\alpha \rightarrow -Q_\alpha$ reflections. Thanks to these symmetries, we can reduce the momentum-space integration to the one-eighth subdomain Ω defined previously, obtaining Eq. (1), which is the second fundamental result of the present paper.

The integral in Eq. (1) extending over one eighth of the reciprocal space can be evaluated numerically, as discussed in the next section. While for the conservative

crystal Eq. (25) predicts that only the phonon modes whose \mathbf{Q} satisfies the resonance condition (23) contribute to friction, the main novelty for the dissipative crystal is that Eq. (1) gathers friction contributions from *all* \mathbf{Q} points. Certainly, the distribution $\mathcal{L}(\mathbf{Q}, v_{\text{SL}}, \gamma)$, Eq. (28), gives more weight to contributions from the \mathbf{Q} -space regions near the S_λ surfaces satisfying Eq. (23) than to more remote regions. In the limit $\gamma \rightarrow 0$ the antiresonant term in Eq. (28) vanishes, and the integral focuses sharply onto the S_λ^Ω surfaces, recovering the result (25) valid for infinite-lifetime phonons.

Equation (1) makes explicit predictions for the friction force originated from weak phonon emission of a point slider crossing a weakly damped harmonic crystal at arbitrary velocity. The resulting friction force can be compared directly against numerical simulations, and in principle even against actual channeling experiments.

V. EVALUATION OF FRICTION

In this section we report the results of the evaluation of the main expression of the present work, Eq. (1), for specific choices of the parameters of the 3D model. We focus on the dissipative crystal for 2 very practical reasons: (i) The alternative evaluation of Eq. (25) would require an accurate numerical determination of the S_λ surfaces, their parameterization, and the implementation of an appropriate surface-integration algorithm. While this is certainly feasible, it is a rather cumbersome task, highly prone to numerical instabilities and implementation mistakes. (ii) It would be practically very difficult, or outright impossible, to compare the resulting friction force with a dissipation-free simulated MD mechanical model. Indeed sliding in a finite-size conservative crystal would progressively heat it up, with temperature and thus friction drifting systematically in time, thus making a steady state unreachable.

For definiteness, we focus on the $T \rightarrow 0$ limit, thus leaving any temperature effects out. In this limit the mean phonon numbers $n_\lambda(\mathbf{k})$ vanish. Consequently the expression Eq. (C11) for the Debye-Waller factor simplifies to

$$W(\mathbf{Q}) = \frac{1}{2N} \sum_{\mathbf{k}, \lambda} |\mathbf{Q} \cdot \boldsymbol{\epsilon}_\lambda(\mathbf{k})|^2 \frac{\hbar}{2m\omega_\lambda(\mathbf{k})}, \quad (30)$$

accounting for zero-point motion. The final fraction in Eq. (30) represents the square of the characteristic length of the quantum harmonic oscillator labeled by \mathbf{k}, λ : in practice the squared amplitude of the spatial quantum fluctuations of that phonon mode. For typical phonon frequencies this amplitude is quite small, ≈ 4 pm for the crystal parameters of Table I. Accordingly, for the relatively short $|\mathbf{Q}|$ vectors that dominate the integral in Eq. (1), most individual terms in the summation of Eq. (30) are quite small too. As a result unity is a fair approximation for both Debye-Waller factors: $\exp(-W(\mathbf{Q})) \simeq 1$ and $\exp(-W(\mathbf{Q} + \mathbf{G}_\perp)) \simeq 1$.

In contrast, for large enough $|\mathbf{Q}|$, this approximation fails, especially for soft phonon modes, which are associated with wider fluctuations, leading to Debye-Waller factors deviating from unity. In practice, in this same large- Q region, having assumed a well-behaved slider-crystal potential, the decay of its Fourier transform $\tilde{V}(Q)$, see Eq. (8) and Fig. 3, makes these large- $|\mathbf{Q}|$ contributions to friction, and the associated deviations of the Debye-Waller factors from unity, negligible anyway. If one wished to address a stiffer potential, characterized by slowly decaying Fourier components $\tilde{V}(Q)$, then precisely the large- $|\mathbf{Q}|$ decay of the Debye-Waller factors will ensure the convergence of the Q integration even in such a situation.

According to this analysis, in the following we substitute unity in place of the Debye-Waller factors of Eq. (1). Observe that in this low-temperature gentle-interaction regime where the Debye-Waller factors approach unity,

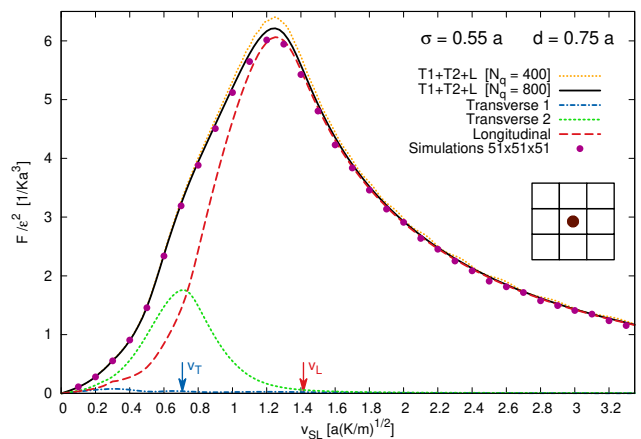


FIG. 4: Friction force as a function of the slider velocity, computed according to Eq. (1), with the slider following the line through the cube centers of the sc lattice, as determined by the initial condition $\mathbf{x}_0 = \frac{a}{2}(\mathbf{e}_y + \mathbf{e}_z)$. The slider-crystal interaction potential, Eq. (8), is parameterized by $\sigma = 0.55a$ and $d = 0.75a$. The second-neighbor spring constant $K' = K/2$, and the crystal is damped by a viscous friction with $\gamma = 0.2(K/m)^{1/2}$. Black solid line: the total friction. Other curves: the contributions of individual polarization branches. Points: friction evaluated by means of numerical simulations. Arrows: the longitudinal (red) and transverse (blue) speeds of sound in the (100) direction.

Planck's constant \hbar disappears from the friction expression altogether, indicating that no quantum effects should be relevant in the present high-velocity, essentially harmonic-crystal conditions – the damping γ assumed to be accordingly small.

A larger damping rate γ makes the Lorentzian weight a smoother function of \mathbf{Q} , which in turn makes the convergence of the integration in Eq. (1) faster, as the \mathbf{Q} -space grid is refined. In contrast, small γ determines a rapidly varying integrand function and, as observed above, concentrates most integration weight sharply around the S_λ surfaces: a converged integral evaluation requires a very fine \mathbf{Q} -space sampling, but comes with the bonus of providing finer details of the velocity dependence of friction. As a fair compromise, for the numerical evaluation of Eq. (1), we adopt an intermediate damping rate $\gamma = 0.2(K/m)^{1/2}$ which makes the Lorentzian broadening factor smooth enough for a feasible numerical integration.

The dispersion relations and the polarization vectors are obtained by solving the secular equation (A1) numerically. Regarding the interaction potential, we fix $\sigma = 0.55a$ and $d = 0.75a$, as depicted in Fig. 3. As the friction force is proportional to ε^2 , in the following we report friction divided by this perturbatively small quantity.

We construct a suite of python programs for executing the integration and summations indicated in Eq. (1). We execute the \mathbf{Q} integration over a wide cubic trun-

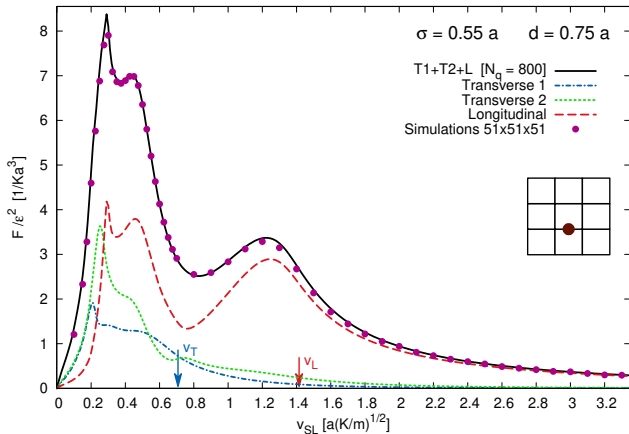


FIG. 5: Same as Fig. 4, but with the slider following the line midway between two rows of atoms, i.e. through nearest-neighbor bond centers of the sc lattice, as dictated by the initial condition $\mathbf{x}_0 = \frac{a}{2} \mathbf{e}_y$.

cation of the region Ω , limiting each component to $0 \leq Q_\alpha \leq Q^{\max} = 2\pi/d_x$. This truncation is consistent with a real-space spatial resolution d_x . We adopt $d_x = 0.15a$, a value that extends the \mathbf{Q} -integration region up to $Q^{\max} \simeq 41.7a^{-1}$. We have verified that, thanks to the rapid decay of the Fourier transform of the potential (Fig. 3) the results are weakly affected by this cutoff. For the integration, each component is sampled on a uniform grid of spacing $\Delta Q = Q^{\max}/N_Q$, with $N_Q = 800$. This grid fineness parameter is the most delicate one for the convergence of the integration in Eq. (1). As for the \mathbf{G}_\perp summation, we include terms with $-l_{\max} \leq l_{x,y} \leq l_{\max}$, with $l_{\max} = 15$: we have verified that friction changes negligibly if we repeat the calculation with $l_{\max} = 10$. The code pre-computes all v_{SL} -independent relevant quantities in Eq. (1) at all \mathbf{Q} grid points and stores them in a set of files. This trick allows us to then execute, for each v_{SL} , the discrete summation representing the \mathbf{Q} integration much more quickly, since just the $\mathcal{L}(\mathbf{Q}, v_{\text{SL}}, \gamma)$ factor is left to evaluate.

Figures 4 and 5 report the result of the numerical integration of Eq. (1) for the channeling trajectories fixed by $\mathbf{x}_0 = \frac{a}{2}(\mathbf{e}_x + \mathbf{e}_y)$ and $\mathbf{x}_0 = \frac{a}{2}\mathbf{e}_x$, respectively. Observe that the velocity dependence is significantly different when the sliding particle follows the two alternative channeling lines, with friction peaking at different velocities. In both figures, the contributions of the three phonon branches to friction are reported individually, showing that for small speed $v_{\text{SL}} < v_{\text{T}}$, longitudinal and transverse phonons contribute in similar proportions,

while for larger speeds the longitudinal phonons dominate.

Importantly, both figures report the comparison of the analytic evaluation of the total friction (black solid curve) according to Eq. (1) with the outcome of MD simulations (pink dots), detailed in Appendix D. The agreement is striking. Small deviations can be traced to the imperfect convergence of the integration grid. The comparison of the $N_q = 800$ curve with the less-converged $N_q = 400$ curve (orange dotted curve of Fig. 4) shows that the finer grid improves the agreement.

In comparing Fig. 5 to Fig. 4, observe that friction peaks at larger values at small velocities when the slider follows the bond-center path. The reason is that the slider approaches the crystal particles more closely (nearest approach distance $a/2$) than along the cube-center path, where the nearest-approach distance equals $a/\sqrt{2}$. At the closer approach distance, the repulsive region $r < \sigma = 0.55a$ of the interaction potential, Fig. 2, begins to get involved, exciting phonons more effectively than the smoother attractive tail.

A. An approximate expression

Since the evaluation of Eq. (1) requires a relatively cumbersome integration, a simpler approximate expression for a quick order-of-magnitude estimation of friction could be of some value. We simplify Eq. (1) by (i) omitting the \mathbf{G}_\perp and λ summations; (ii) replacing each \mathbf{Q} component with d^{-1} (thus $|\mathbf{Q}| \rightarrow \sqrt{3}/d$), estimating the region where $\tilde{V}(|\mathbf{Q}|)$ peaks; (iii) substituting the amplitude of the d^3Q integration with the volume $(2\pi/d)^3$ of the \mathbf{Q} -space region where $\tilde{V}(|\mathbf{Q}|)$ is nonnegligible, see Fig. 3; (iv) replacing the polarization vectors ϵ_λ with unity; (v) replacing the Debye-Waller exponentials with unity too:

$$\begin{aligned} F(v_{\text{SL}}) &\approx \frac{4\pi}{ma^3} \frac{1}{d^3} d^{-1} \tilde{V}^2 \left(\frac{\sqrt{3}}{d} \right) d^{-2} \mathcal{L}(d^{-1}\hat{\mathbf{x}}, v_{\text{SL}}, \gamma) \\ &= \frac{4\pi}{ma^3} \frac{\tilde{V}^2 \left(\frac{\sqrt{3}}{d} \right)}{d^6} \mathcal{L}(d^{-1}\hat{\mathbf{x}}, v_{\text{SL}}, \gamma). \end{aligned} \quad (31)$$

To estimate the velocity-dependent \mathcal{L} factor defined in Eq. (29), we introduce a typical phonon frequency $\omega_{\text{ph}} \approx (K'/m)^{1/2} = (K/2m)^{1/2}$ and a scaled dimensionless slider velocity $w = v_{\text{SL}}/(d\omega_{\text{ph}})$. In terms of these quantities, we estimate \mathcal{L} as follows:

$$\begin{aligned} \mathcal{L}(d^{-1}\hat{\mathbf{x}}, v_{\text{SL}}, \gamma) &\approx \frac{\gamma}{2\pi} \frac{4d^{-1}v_{\text{SL}}}{[(d^{-1}v_{\text{SL}} - \omega_{\text{ph}})^2 + (\frac{\gamma}{2})^2][(d^{-1}v_{\text{SL}} + \omega_{\text{ph}})^2 + (\frac{\gamma}{2})^2]} \\ &= \frac{2\gamma}{\pi \omega_{\text{ph}}^3} \frac{w}{[(w-1)^2 + (\frac{\gamma}{2\omega_{\text{ph}}})^2][(w+1)^2 + (\frac{\gamma}{2\omega_{\text{ph}}})^2]}, \end{aligned} \quad (32)$$

providing a typical order of magnitude. The ratio $\gamma/(2\omega_{\text{ph}})$ is inversely related to the quality factor of a typical phonon oscillator. For \mathcal{L} , the expression (32) provides a fair off-resonance ($w \ll 1$ or $w \gg 1$) estimation, and even for speeds matching a phonon resonance ($w = 1$). The product $v_s = a\omega_{\text{ph}}$ represents a typical sound velocity of the order of the speeds of sound evaluated in Appendix A. In terms of these quantities, by combining Eqs. (31) and (32), the order of magnitude of the off-resonance friction force is

$$\begin{aligned} F &\approx \frac{8\gamma}{mv_s^3} \frac{\tilde{V}^2\left(\frac{\sqrt{3}}{d}\right)}{d^6} \times \\ &\quad \frac{w}{[(w-1)^2 + (\frac{\gamma}{2\omega_{\text{ph}}})^2][(w+1)^2 + (\frac{\gamma}{2\omega_{\text{ph}}})^2]} \quad (33) \\ &\approx \frac{8\gamma}{mv_s^3} \frac{\tilde{V}^2\left(\frac{\sqrt{3}}{d}\right)}{d^6} \times \begin{cases} \frac{w}{\left[1 + \left(\frac{\gamma}{2\omega_{\text{ph}}}\right)^2\right]^2} & \text{for } w \ll 1 \\ \frac{1}{\left(\frac{\gamma}{2\omega_{\text{ph}}}\right)^2 \left[2 + \left(\frac{\gamma}{2\omega_{\text{ph}}}\right)^2\right]} & \text{for } w = 1 \\ \frac{1}{w^3} & \text{for } w \gg 1 \end{cases} \end{aligned}$$

This expression is proportional to the square of the coupling energy $\varepsilon \propto \tilde{V}(\sqrt{3}/d)/d^3$, as expected of a linear-response result.

Figure 6 compares the estimation of Eq. (33) with the full Eq. (1) and with numerical simulations over a broad velocity range explored in logarithmic scale. It is seen that the order-of-magnitude estimation Eq. (33) yields a weak friction $\propto v_{\text{SL}}$ for $v_{\text{SL}} \rightarrow 0$, a peaking friction related to the square of the typical quality factor of phonon oscillators at intermediate speed, and a rapidly decaying friction $\propto v_{\text{SL}}^{-3}$ in the large- v_{SL} limit. The rough estimation Eq. (33) is in fair qualitative agreement with the exact formula Eq. (1), with the correct power-law asymptotic dependences and a roughly positioned friction peak, but shows of course significant quantitative deviations, especially at low velocity.

Interestingly, the fact that the approximate formula depends on v_{SL} through the dimensionless ratio $w = v_{\text{SL}}/(d\omega_{\text{ph}})$ suggests that relevant speed to which v_{SL} should be compared is not the speed of sound v_s , but rather the combination $d\omega_{\text{ph}}$ of the characteristic length scale of the slider-crystal interaction and the typical vibration frequency of the crystal.

The nearly perfect agreement of Eq. (1) with the simulations in the velocity range around the speeds of sound degrades somewhat at higher velocity. This is due to multiple effects including: (i) the truncation of the \mathbf{Q}

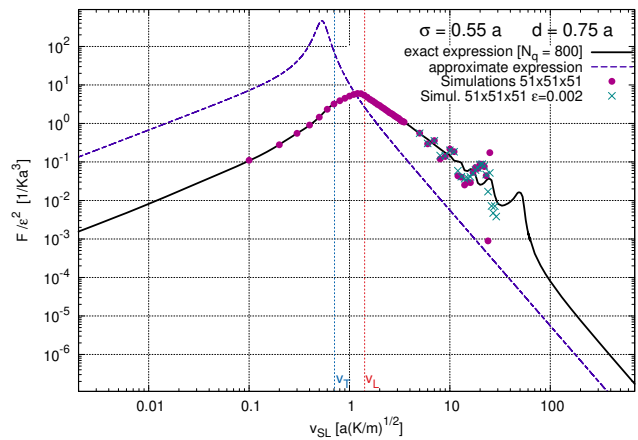


FIG. 6: A broad-range comparison of the total friction force as a function of the slider velocity, computed according to Eq. (1) (solid), with the approximate expression (33) (dashed), for the same conditions and parameters as in Fig. 4. Points: friction evaluated by means of numerical simulations carried out with coupling $\varepsilon = 5 \times 10^{-4} Ka^2$ (circles) or $\varepsilon = 0.002 Ka^2$ (crosses). Vertical dashed lines: the longitudinal (red) and transverse (blue) speeds of sound in the (100) direction.

integration to a finite cutoff Q^{max} affects the wiggles of the theory curve; (ii) the very low friction in this region makes its numeric evaluation through simulations prone to roundoff error, which we reduce by repeating the calculation with a larger coupling (cross points in Fig. 6).

VI. THE 2D MODEL

It is instructive to adapt the results obtained for the 3D crystal to a 2D square lattice. First off, we turn all vector quantities into 2D vectors. For the 2D crystal the integration domain Ω of Eq. (22) is replaced by its 2D version, namely the quadrant ($Q_x \geq 0, Q_y \geq 0$). The polarization index λ takes only two values for the transverse and longitudinal phonon branches. The sum over \mathbf{G}_{\perp} involves just the y component:

$$\mathbf{G}_{\perp} = \left(0, \frac{2\pi}{a} l_y\right)$$

associated to a single Miller index l_y . In adapting Eq. (22) to 2D, a power of a , a factor 2π at the denominator, and a factor 2 at the numerator originated by

symmetry must also be removed. According to these observations, the 2D version of Eq. (22), valid for infinitely-

long-lived phonons, is

$$F(v_{\text{SL}}) = \frac{2\pi}{ma^2} \sum_{l_y} (-1)^{l_y} \int_{\Omega} \frac{d^2Q}{(2\pi)^2} Q_x \tilde{V}(|\mathbf{Q}|) \tilde{V}(|\mathbf{Q} + \mathbf{G}_y|) e^{-W(\mathbf{Q}) - W(\mathbf{Q} + \mathbf{G}_y)} \times \sum_{\lambda} \frac{\mathbf{Q} \cdot \boldsymbol{\epsilon}_{\lambda}(\mathbf{Q}) (\mathbf{Q} + \mathbf{G}_y) \cdot \boldsymbol{\epsilon}_{\lambda}(\mathbf{Q})}{\omega_{\lambda}(\mathbf{Q})} \delta(\mathbf{Q} \cdot \mathbf{v}_{\text{SL}} - \omega_{\lambda}(\mathbf{Q})). \quad (34)$$

We can reformulate the 2D integral, using the following property of the Dirac delta:

$$\int_{\Omega} d^2Q g(\mathbf{Q}) \delta(f(\mathbf{Q})) = \int_{\ell^{\Omega}} dQ \frac{g(\mathbf{Q})}{|\nabla f(\mathbf{Q})|}, \quad (35)$$

where ℓ^{Ω} is the curve consisting of the solutions of the equation $f(\mathbf{Q}) = 0$ in the \mathbf{Q} -space domain Ω . Specifically for Eq. (34) we take

$$f(\mathbf{Q}) = \mathbf{Q} \cdot \mathbf{v}_{\text{SL}} - \omega_{\lambda}(\mathbf{Q}) = Q_x v_{\text{SL}} - \omega_{\lambda}(\mathbf{Q}), \quad (36)$$

and therefore

$$\nabla f(\mathbf{Q}) = \mathbf{v}_{\text{SL}} - \mathbf{v}_{\lambda}(\mathbf{Q}) = \begin{pmatrix} v_{\text{SL}} - v_{\lambda x}(\mathbf{Q}) \\ -v_{\lambda y}(\mathbf{Q}) \end{pmatrix}. \quad (37)$$

Like in 3D, we introduce the group velocity of the phonons $\mathbf{v}_{\lambda}(\mathbf{Q}) = \nabla \omega_{\lambda}(\mathbf{Q})$, namely the gradient of their dispersion, with components $v_{\lambda x/y}(\mathbf{Q})$. For each polarization λ , the solution of $Q_x v_{\text{SL}} = \omega_{\lambda}(\mathbf{Q})$ generates a specific curve ℓ_{λ}^{Ω} .

Substituting these relations into Eq. (34), we obtain the 2D analogous of Eq. (25):

$$F(v_{\text{SL}}) = \frac{2\pi}{ma^2} \sum_{l_y} (-1)^{l_y} \sum_{\lambda} \int_{\ell_{\lambda}^{\Omega}} \frac{dQ}{(2\pi)^2} Q_x \tilde{V}(|\mathbf{Q}|) \tilde{V}(|\mathbf{Q} + \mathbf{G}_{\perp}|) e^{-W(\mathbf{Q}) - W(\mathbf{Q} + \mathbf{G}_{\perp})} \frac{\mathbf{Q} \cdot \boldsymbol{\epsilon}_{\lambda}(\mathbf{Q}) (\mathbf{Q} + \mathbf{G}_{\perp}) \cdot \boldsymbol{\epsilon}_{\lambda}(\mathbf{Q})}{\omega_{\lambda}(\mathbf{Q}) |\mathbf{v}_{\text{SL}} - \mathbf{v}_{\lambda}(\mathbf{Q})|}. \quad (38)$$

The denominator $|\mathbf{v}_{\text{SL}} - \mathbf{v}_{\lambda}(\mathbf{Q})|$ vanishes at the special slider speeds, that, in addition to Eq. (23), match the ‘‘shock wave’’ condition (26). In 2D this condition requires that both components of the group velocity $\mathbf{v}_{\lambda}(\mathbf{Q})$ match those of the slider velocity

$$v_{\lambda x}(\mathbf{Q}) \equiv \frac{\partial \omega_{\lambda}(\mathbf{Q})}{\partial Q_x} = v_{\text{SL}}, \quad (39)$$

$$v_{\lambda y}(\mathbf{Q}) \equiv \frac{\partial \omega_{\lambda}(\mathbf{Q})}{\partial Q_y} = 0. \quad (40)$$

The vanishing denominator $|\mathbf{v}_{\text{SL}} - \mathbf{v}_{\lambda}(\mathbf{Q})|$ gives the friction force an especially large singular contribution. Like the Van Hove singularities in the density of the electronic states and of the harmonic phonon frequencies,¹¹ in the 1D model a similar singularity in the force integration led to peaks with diverging friction;⁶ in the 2D model at hand these singularities generate friction peaks char-

acterized by a jump in the first derivative dF/dv_{SL} ; in 3D they lead to smoother and milder friction peaks, as shown in Figs. 4 and 5.

For the square-lattice phonon dispersions at hand, the condition (40) is verified only for $Q_y = n\pi/a$, for integer n , indicating that shock-wave contributions, if any, can arise only along these special symmetry lines. As for the Q_x component, locations where also condition (39) is fulfilled occur within suitable v_{SL} ranges: in particular, for small Q_x and supersonic slider speed the shockwave condition (39) is certainly *not* met. Instead, this condition is met at larger and larger special Q_x values, corresponding to smaller and smaller special v_{SL} values. Geometric examples of matching the shockwave condition (39) are illustrated in Fig. 7 for even n , and in Fig. 8 for odd n .

As was done for the 3D model with Eq. (1), the introduction of a finite-phonon-lifetime γ replaces the Dirac deltas with Lorentzian peaks, yielding

$$F(v_{\text{SL}}) = \frac{2\pi}{ma^2} \sum_{l_y} (-1)^{l_y} \int_{\Omega} \frac{d^2Q}{(2\pi)^2} Q_x \tilde{V}(|\mathbf{Q}|) \tilde{V}(|\mathbf{Q} + \mathbf{G}_{\perp}|) e^{-W(\mathbf{Q}) - W(\mathbf{Q} + \mathbf{G}_{\perp})} \times \sum_{\lambda} \mathbf{Q} \cdot \boldsymbol{\epsilon}_{\lambda}(\mathbf{Q}) (\mathbf{Q} + \mathbf{G}_{\perp}) \cdot \boldsymbol{\epsilon}_{\lambda}(\mathbf{Q}) \mathcal{L}(\mathbf{Q}, v_{\text{SL}}, \gamma), \quad (41)$$

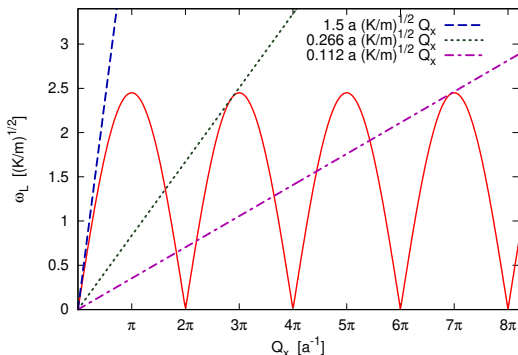


FIG. 7: Solid curve: the longitudinal phonon dispersion for the 2D simple-cubic crystal along the $Q_y = 0$ line in a repeated-zone scheme. Dashed line: the straight line whose slope is a supersonic speed $v_{\text{SL}} = 1.5 a(K/m)^{1/2} > v_{\text{L}}^{2\text{D}}$ never intersects the dispersion curve. Other straight lines with slope $v_{\text{SL}} = 0.266 a(K/m)^{1/2}$ (dotted) and $v_{\text{SL}} = 0.112 a(K/m)^{1/2}$ (dot-dashed) are examples of speeds that meet the shockwave tangency conditions (39) and (40). Note that a smaller v_{SL} leads to a tangency point at a larger Q_x .

where $\mathcal{L}(\mathbf{Q}, v_{\text{SL}}, \gamma)$ is defined in Eq. (29). Expression (41) is the 2D analogue of Eq. (1), and is similarly ready to be evaluated numerically.

A. Comparison with simulations

Like in the 3D model we evaluate friction in the zero-temperature limit, replacing the Debye-Waller factors with unity. Like in Sect. V, \hbar drops out of the expression, thus our theory predicts negligible quantum effect in this limit.

Even though the dispersion relation is available analytically, see Eq. (A4), in the code we compute $\omega_{\lambda}(\mathbf{Q})$ and the corresponding polarization vectors $\boldsymbol{\epsilon}_{\lambda}$ by diagonalizing numerically the 2×2 dynamical matrix defined by Eqs. (A2) and (A3), setting $K' = K/2$. Like for the 3D model, in the figures below we report the friction force F divided by the square of the perturbatively small coupling energy ε .

The code for the 2D model follows the same strategy as the 3D code, with the same real-space resolution $d_x = 0.15a$ as in 3D. For the integration grid we can afford a spacing $\Delta Q = Q^{\text{max}}/N_Q$, with $N_Q = 2500$, far finer than in 3D. Thanks to this finer grid, we can adopt a smaller damping rate $\gamma = 0.05 (K/m)^{1/2}$, allowing us to

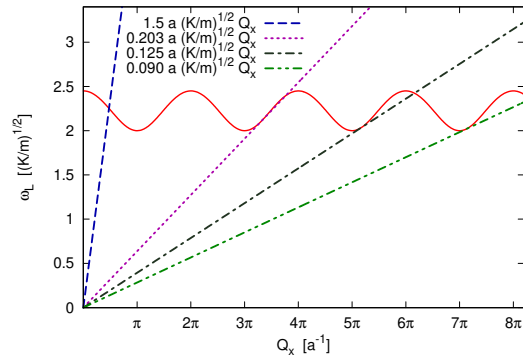


FIG. 8: Same as Fig. 7, but along the $Q_y = \pi/a$ line. Dashed line: the straight line at supersonic speed $v_{\text{SL}} = 1.5 a(K/m)^{1/2}$ intersects the dispersion curve, but never meets the tangency condition (39). Other straight lines with slope $v_{\text{SL}} \simeq 0.203 a(K/m)^{1/2}$ (dotted), $v_{\text{SL}} \simeq 0.125 a(K/m)^{1/2}$ (dot-dashed), and $v_{\text{SL}} \simeq 0.090 a(K/m)^{1/2}$ (dot-dot-dashed) provide examples of speeds for which the shockwave tangency conditions are met.

investigate the velocity dependence of friction in greater detail. For the \mathbf{G}_{\perp} summation, we consider $-15 \leq l_y \leq 15$. We verified that, thanks to the rapid decay of the Fourier transform of the potential and the smoothness of the integrand function, the evaluated friction force does not change visibly if these truncation limits and the grid fineness are improved.

Figure 9 compares the friction force obtained from the evaluation of Eq. (41) (solid curve) with that obtained by MD simulations (circles), executed with the same parameters considered for the analytic expression, as detailed in Appendix D. The qualitative and quantitative agreement is striking. The analytic expression (41) reproduces the MD simulation result in all its detailed structure at all velocities, except for small deviations at the lowest ones. The red dot-dashed and blue dashed curves report the separate contributions of the longitudinal and transverse phonons. The longitudinal phonons dominate friction across the velocity range, except at relatively low velocity $v_{\text{SL}} < 0.2 a(K/m)^{1/2}$ and $0.6 a(K/m)^{1/2} < v_{\text{SL}} < 0.7 a(K/m)^{1/2}$.

Friction exhibits a sharp peak, labeled “1” in Fig. 9, at $v_{\text{SL}} = 0.203 a(K/m)^{1/2}$. As demonstrated by the dotted line in Fig. 8, this is precisely the speed matching a tangency shockwave condition for the longitudinal phonon, but with substantial contributions from the transverse phonons, too.

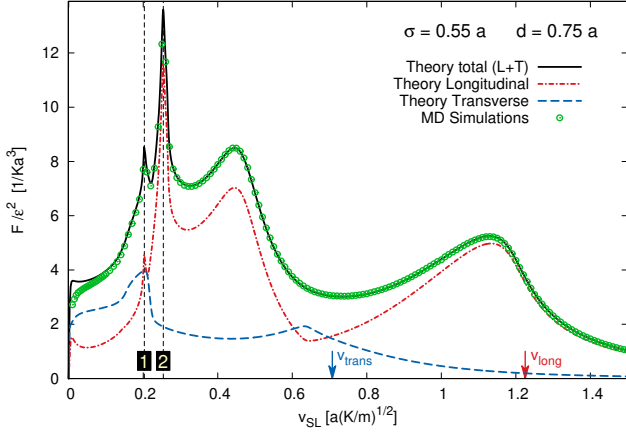


FIG. 9: Comparison of the slider-speed dependence of the friction force F obtained evaluating the 2D LR expression (41) (solid curve), with that obtained by numerical MD simulations based on a crystal of 201×201 atoms, see Appendix D for details. Dashed and dot-dashed curves: the contributions to the total friction of the transverse and longitudinal phonons, respectively. Thin vertical dashed lines labeled 1 and 2: the speeds where friction peaks for reasons discussed in the text. The reported friction force is divided by ε^2 , expressing the strength of the slider-crystal interaction potential, Eq. (7). In both theory and simulations, a damping rate $\gamma = 0.05 (K/m)^{1/2}$ is applied.

The next, even stronger, friction peak labeled “2” at $v_{\text{SL}} = 0.2535 a(K/m)^{1/2}$, marked by a vertical thin dashed line, does *not* result from a shockwave point instead, because at this velocity the tangency conditions (39) and (40) are fulfilled nowhere in \mathbf{Q} space, see Figs. 7 and 8. We can rather understand this peak as generated by a relatively broad region of \mathbf{Q} satisfying approximately the resonance condition (23) for the longitudinal phonon dispersion near $\mathbf{Q} \simeq (2.6, 0.49) \frac{\pi}{a}$, see Fig. 10. Although resonant matching is not exact, the adopted Lorentzian broadening makes the factor $\mathcal{L}(\mathbf{Q}, v_{\text{SL}}, \gamma)$ in Eq. (41) quite large over this wide \mathbf{Q} region, contributing to make friction peak 2 so strong.

This same mechanism of an extended region of approximate resonance contributes to the intensity of peak 1, but instead lacks for the other shockwave resonances shown in Figs. 7 and 8. This explains why these other resonances do not produce visible peaks for the considered phonon broadening. If one could decrease γ , thus approaching the conservative-crystal limit $\gamma \rightarrow 0$, one would observe the appearance of multiple sharp (albeit relatively weak) shockwave peaks; at the same time the nonresonant peak 2 would progressively lose its prominence.

Figure 11 reports the friction force evaluated through Eq. (9), but with a different slider-crystal interaction $V(r)$, defined by $\sigma = 0.55 a$ and $d = 0.9 a$, shown in Fig. 2. The accord between theory and simulations as remarkable as for the other interaction. Observe that friction is weaker overall, and that the speeds of fric-

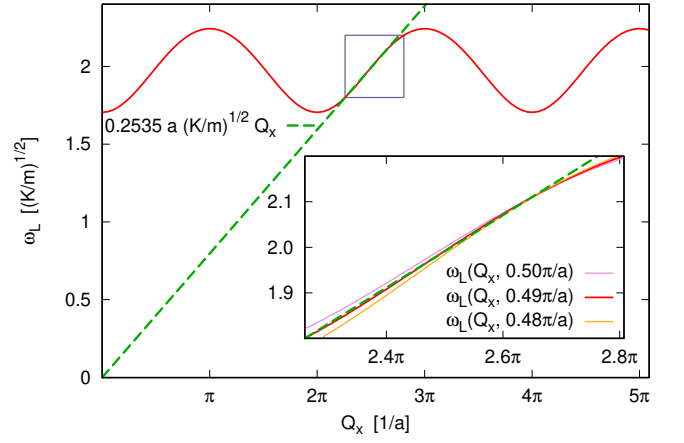


FIG. 10: Solid line: longitudinal phonon dispersion along the line $Q_y \equiv 0.49 \frac{\pi}{a}$, compared to the straight line with slope $v_{\text{SL}} = 0.2545 a(K/m)^{1/2}$ (dashed). Inset: a blowup of the close-approach region, illustrating how the straight line associated to this specific speed comes extraordinarily close to the phonon dispersion over a sizable range of Q_x and Q_y values. This approach is very close to satisfying the resonance condition (23), but not the shockwave condition, and specifically not Eq. (40), which holds at $Q_y = n \frac{\pi}{a}$ only.

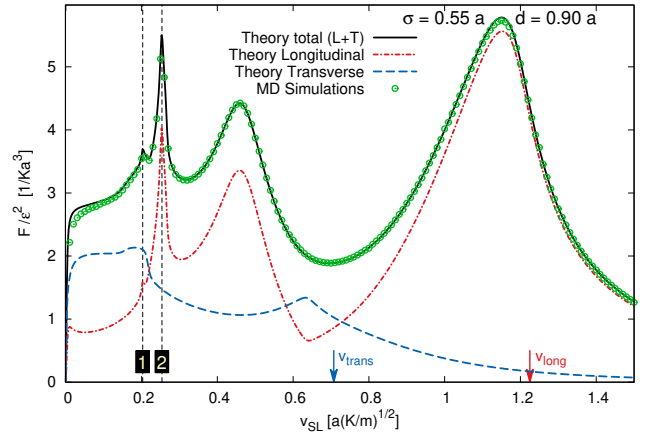


FIG. 11: Same as Fig. 9, but for a different slider-crystal interaction, defined by $\sigma = 0.55 a$ and $d = 0.9 a$. Note that the friction peaks labeled 1 and 2 occur at the same speeds $v_{\text{SL}} = 0.203 a(K/m)^{1/2}$ and $v_{\text{SL}} = 0.2535 a(K/m)^{1/2}$, as in Fig. 9. This is expected, since the peaks positions only depend on the phonon dispersion, not on the slider-crystal interaction, which is the only different ingredient for the two graphs. In contrast, the relative fractional contributions to friction of longitudinal and transverse phonons, as well as the absolute friction value, are significantly affected by changes in $V(r)$.

tion peaks 1 and 2 are the same as in the calculation done with a different potential, reported in Fig. 9. This outcome is precisely predicted by our theory, which has friction peaks at velocities that depend uniquely on the phonon dispersion, and not on the slider-crystal interaction. Even though the peak position are preserved, the

detailed dependence of friction on velocity is seen as a sensitive function of the interaction potential.

VII. DISCUSSION AND CONCLUSION

Based on quantum linear-response (LR) theory complemented by well-understood approximations, we bring the theory of kinetic friction of a particle interacting with a periodic surrounding in the weak-interaction regime to an analytic formula, which is both formally instructive and practically useful. We derive concrete implementations of the general expression for particle channeling through two models of harmonic crystals: (i) a 3D simple-cubic crystal, and (ii) a 2D square lattice.

For both models, we provide a physical decomposition of the friction force into an integration and a summation of products of the equilibrium dynamical response of the unperturbed crystal (a quantity depending uniquely on the crystal phonon dispersions and polarizations and on temperature) times the slider-crystal interaction in Fourier space. This formulation shows that the advancing slider preferentially excites those phonons that match the resonance condition Eq. (23), which are therefore identified as the main responsible for energy dissipation.

We compared the 3D and 2D expressions with the friction evaluated by means of MD simulations. The remarkably close match serves as a validation of the analytical results.

Beside providing a conceptual understanding of the microscopic friction mechanism, the analytical formulation has obvious advantages over using MD simulations to simulate friction. For each sliding speed, the analytical friction calculation requires the numerical evaluation of an integral, a task computationally far cheaper than setting up and running a full-fledged numerical simulation. Additionally, the analytic result addresses directly the thermodynamic limit of a macroscopically large crystal, while simulations are confronted by size and time limitations, which could prove rather difficult to control, especially for 3D crystals.

The present results, though remarkable, are limited in scope by two main assumptions: (i) an infinite crystal, and (ii) a weak particle-crystal interaction. The first assumption implies the rather idealized channeling geometry, as opposed to the more conventional contact-to-surface geometry, as, e.g., in ordinary atomic-force-microscopy (AFM) experiments.

As it stands, our theory for the energy loss in channeling could apply e.g. to the slowing of neutral particles,²⁸ e.g. fast neutrons channeled across crystals.^{12–15} A reader who wished to apply the present theory to compute the energy loss of channeled neutrons, though, should be warned that the extremely short-range nature of the neutron-nucleus interaction would make the FT $\tilde{V}(q)$ for that problem decay extremely slowly. In turn, this would make the numerical \mathbf{Q} integration in Eq. (1) more challenging, and relying explicitly on the regularization pro-

vided by the large- $|\mathbf{Q}|$ decay of the Debye-Waller factors.

To address the more practical problem of evaluating sliding friction in a real-life contact-to-surface geometry, the next step is a generalization of this theory to the sliding in contact with a semi-infinite 3D crystal. For this extension, one specific complication will be the need to describe surface phonons accurately, due to their likely relevant role for dissipation. It may be possible to address this problem by a suitable adaptation of techniques such as the one used in Ref. 16. Further applications could require extension of this theory to general crystals and to non-crystalline solids, where not all simplifications based on symmetry used in the present work will be applicable.

The second main assumption, that of weak coupling, is appropriate for noncontact AFM experiments. It will be important to overcome this limit when using this approach to address e.g. contact-mode AFM, in strong-friction conditions, where stick-slip dynamics arises. Perhaps a Dyson-like resummation approach¹⁷ could allow us to extend this theory beyond LR. Further aspects that call for future attention are temperature and quantum effects in the simulations, plus phonon anharmonicity to replace the phenomenological damping γ in the theory. These effects are nevertheless expected to be much more important for low-speed, stick-slip friction than in the present case.

Acknowledgments

We acknowledge useful discussion and feedback from Emanuele Panizon. E.T. and G.E.S. acknowledge that the research was partly supported by EU Horizon 2020 under ERC-ULTRADISS, Grant Agreement No. 834402. G.E.S. acknowledges financial support from PNRR MUR project PE0000023-NQSTI, from PRIN 2022H77XB7 of the Italian Ministry of University and Research, and from the QuantERA II Programme STAQS project that has received funding from the European Union's H2020 research and innovation programme under Grant Agreement No 101017733. G.E.S. acknowledges that his research has been conducted within the framework of the Trieste Institute for Theoretical Quantum Technologies (TQT).

Appendix A: The lattice phonons and their symmetries

Our model elastic crystal consists of point particles with mass m that at equilibrium are arranged as a square (2D) or simple-cubic (3D) lattice. Harmonic nearest- and second-neighbor (diagonal) springs with, respectively, elastic constants K and K' and equilibrium lengths a and $\sqrt{2}a$ guarantee the mechanical stability and determine the phonon properties.

The phonon polarization vectors $\epsilon_\lambda(\mathbf{q})$ and frequencies $\omega_\lambda(\mathbf{q})$ are obtained by diagonalizing the dynamical ma-

trix $D_{\mu\nu}(\mathbf{q})$. For these monoatomic crystals, the eigenvalue equation

$$\omega_\lambda^2(\mathbf{q})\epsilon_{\lambda\mu}(\mathbf{q}) = \sum_\nu D_{\mu\nu}(\mathbf{q})\epsilon_{\lambda\nu}(\mathbf{q}) \quad (\text{A1})$$

involves a 2×2 (2D) or 3×3 (3D) matrix.

In 2D, the dynamical matrix has the following diagonal ($\mu\mu$) and off-diagonal ($\mu\nu$) elements:

$$D_{\mu\mu}(\mathbf{q}) = \frac{2K}{m} [1 - \cos(q_\mu a)] + \frac{2K'}{m} [1 - \cos(q_\mu a) \cos(q_\nu a)], \quad (\text{A2})$$

$$D_{\mu\nu}(\mathbf{q}) = \frac{2K'}{m} \sin(q_\mu a) \sin(q_\nu a), \quad (\text{A3})$$

with $\mu, \nu = x, y$ and $\nu \neq \mu$.

From the secular equation (A1) we obtain the dispersion relations:

$$\omega_\pm(\mathbf{q}) = \left\{ 2\frac{K}{m} \left[\sin^2\left(\frac{q_x a}{2}\right) + \sin^2\left(\frac{q_y a}{2}\right) + \frac{K'}{K} (1 - \cos(q_x a) \cos(q_y a)) \right] \pm 2\frac{K}{m} \left[\left(\sin^2\left(\frac{q_x a}{2}\right) - \sin^2\left(\frac{q_y a}{2}\right) \right)^2 + \left(\frac{K'}{K} \sin(q_x a) \sin(q_y a) \right)^2 \right]^{1/2} \right\}^{1/2}, \quad (\text{A4})$$

for the $\lambda = 1$ transverse (-) and $\lambda = 2$ longitudinal (+) phonons. The (isotropic) transverse and longitudinal speeds of sound are

$$v_{\text{T}}^{2\text{D}} = a \left(\frac{K'}{m} \right)^{1/2} \left[= \frac{1}{\sqrt{2}} a \left(\frac{K}{m} \right)^{1/2} \right], \quad (\text{A5})$$

$$v_{\text{L}}^{2\text{D}} = a \left(\frac{K + K'}{m} \right)^{1/2} \left[= \sqrt{\frac{3}{2}} a \left(\frac{K}{m} \right)^{1/2} \right], \quad (\text{A6})$$

with the expressions in square brackets corresponding to the adopted ratio $K'/K = \frac{1}{2}$.

Likewise in 3D, the 3×3 dynamical matrix can be expressed as an explicit function of \mathbf{q} . The diagonal elements are:

$$D_{\mu\mu}(\mathbf{q}) = 2\frac{K}{m} [1 - \cos(q_\mu a)] + 2\frac{K'}{m} [2 - \cos(q_\mu a)(\cos(q_\nu a) + \cos(q_\gamma a))] \quad (\text{A7})$$

with $\mu, \nu, \gamma = x, y, z$, $\nu \neq \mu$ and $\gamma \neq \mu, \gamma \neq \nu$.

The 2D expression for the off-diagonal elements (A3) holds in 3D too. Like in 2D, the diagonalization of D provides normal-mode frequencies and phonon polarization vectors for \mathbf{q} spanning the first Brillouin zone. Diagonalization of the small- $|\mathbf{q}|$ expansion of this dynamical matrix determines the sound velocities. At variance with

the 2D case, they depend on the direction of \mathbf{q} . For example in the (100) direction, the transverse and longitudinal speeds of sound are

$$v_{\text{T}}^{3\text{D}} = a \left(\frac{K'}{m} \right)^{1/2} \left[= \frac{1}{\sqrt{2}} a \left(\frac{K}{m} \right)^{1/2} \right], \quad (\text{A8})$$

$$v_{\text{L}}^{3\text{D}} = a \left(\frac{K + 2K'}{m} \right)^{1/2} \left[= \sqrt{2} a \left(\frac{K}{m} \right)^{1/2} \right], \quad (\text{A9})$$

with the expressions in square brackets corresponding to the adopted value $K' = K/2$. For this same condition, in the (111) direction the sound velocities are

$$v_{\text{T}}^{3\text{D}} = \sqrt{\frac{2}{3}} a \left(\frac{K}{m} \right)^{1/2} \quad \text{and} \quad v_{\text{L}}^{3\text{D}} = \sqrt{\frac{5}{3}} a \left(\frac{K}{m} \right)^{1/2},$$

instead.

In both 2D and 3D, the dynamical matrix is explicitly even under inversion $\mathbf{q} \rightarrow -\mathbf{q}$. As a result, $\omega_\lambda(-\mathbf{q}) = \omega_\lambda(\mathbf{q})$. We can also assume that the arbitrary phases of the polarization vectors are fixed in such a way that

$$\epsilon_\lambda(-\mathbf{q}) = \epsilon_\lambda(\mathbf{q}). \quad (\text{A10})$$

Additionally, we derive the symmetry of the polarization vectors under a single-component reflection: $q_\mu \rightarrow -q_\mu$ (the two other components q_ν and q_γ remaining unchanged). We indicate with \mathbf{q}' the vector obtained from \mathbf{q} under this reflection. By analyzing the secular equation (A1) at \mathbf{q}' , we obtain the relevant symmetry relations for the polarization vectors:

$$\begin{aligned} \omega_\lambda^2(\mathbf{q}')\epsilon_{\lambda\mu}(\mathbf{q}') &= D_{\mu\mu}(\mathbf{q}')\epsilon_{\lambda\mu}(\mathbf{q}') + D_{\mu\nu}(\mathbf{q}')\epsilon_{\lambda\nu}(\mathbf{q}') + D_{\mu\gamma}(\mathbf{q}')\epsilon_{\lambda\gamma}(\mathbf{q}') \\ &= D_{\mu\mu}(\mathbf{q})\epsilon_{\lambda\mu}(\mathbf{q}') - D_{\mu\nu}(\mathbf{q})\epsilon_{\lambda\nu}(\mathbf{q}') - D_{\mu\gamma}(\mathbf{q})\epsilon_{\lambda\gamma}(\mathbf{q}') \end{aligned} \quad (\text{A11})$$

with $\gamma \neq \nu \neq \mu \neq \gamma$.

Equation (A11) is satisfied provided that

$$\omega_\lambda(\mathbf{q}') = \omega_\lambda(\mathbf{q}), \quad (\text{A12})$$

and that the corresponding polarization vector components are taken as follow:

$$\begin{aligned} \epsilon_{\lambda\mu}(\mathbf{q}') &= \epsilon_{\lambda\mu}(\mathbf{q}) \\ \epsilon_{\lambda\nu}(\mathbf{q}') &= -\epsilon_{\lambda\nu}(\mathbf{q}), \quad \text{for } \nu \neq \mu. \end{aligned} \quad (\text{A13})$$

This relation (A13) expresses the symmetry of the polarization vectors under reflection in both 3D and 2D: in the calculation of the lattice response function, Appendix C, we rely on this symmetry.

Appendix B: Symmetries of the response function

Here we discuss a few symmetry property of the retarded response function relevant for the calculation of

friction. Consider the Fourier representation of the retarded response function for an arbitrary operator $A = A(\mathbf{r})$. Clearly, if the two momentum arguments are the same, the real part is even and the imaginary part is odd under $\mathbf{Q} \rightarrow -\mathbf{Q}$, namely:

$$\text{Re } \chi_{AA}^R(\mathbf{Q}, \mathbf{Q}, \omega) = \text{Re } \chi_{AA}^R(-\mathbf{Q}, -\mathbf{Q}, \omega) \quad (\text{B1})$$

$$\text{Im } \chi_{AA}^R(\mathbf{Q}, \mathbf{Q}, \omega) = -\text{Im } \chi_{AA}^R(-\mathbf{Q}, -\mathbf{Q}, \omega). \quad (\text{B2})$$

However, for different momenta, as in Eq. (14), no straightforward parity symmetry holds. However, for the specific periodic problem, where the arguments differ by a \mathbf{G} vector, another relevant symmetry property holds.

Consider the Fourier transform of a general correlation function for operator A :

$$\chi_{AA}^R(\mathbf{Q}, \mathbf{Q} + \mathbf{G}, \omega) = \int d^3\mathbf{x} \int d^3\mathbf{x}' \times \quad (\text{B3}) \\ e^{-i\mathbf{Q}\cdot\mathbf{x}} \chi_{AA}^R(\mathbf{x}, \mathbf{x}', \omega) e^{i(\mathbf{Q}+\mathbf{G})\cdot\mathbf{x}'}$$

Add to this expression the corresponding formula with $-\mathbf{G}$ in place of \mathbf{G} :

$$\chi_{AA}^R(\mathbf{Q}, \mathbf{Q} + \mathbf{G}, \omega) + \chi_{AA}^R(\mathbf{Q}, \mathbf{Q} - \mathbf{G}, \omega) = \quad (\text{B4}) \\ = \int d^3\mathbf{x} \int d^3\mathbf{x}' \times \\ e^{-i\mathbf{Q}\cdot\mathbf{x}} \chi_{AA}^R(\mathbf{x}, \mathbf{x}', \omega) \left[e^{i(\mathbf{Q}+\mathbf{G})\cdot\mathbf{x}'} + e^{i(\mathbf{Q}-\mathbf{G})\cdot\mathbf{x}'} \right].$$

If we replace \mathbf{Q} with $-\mathbf{Q}$, the exponential factors at the right hand side turn into their complex conjugate. As a consequence,

$$\chi_{AA}^R(\mathbf{Q}, \mathbf{Q} + \mathbf{G}, \omega) + \chi_{AA}^R(\mathbf{Q}, \mathbf{Q} - \mathbf{G}, \omega) = \quad (\text{B5}) \\ = \left[\chi_{AA}^R(-\mathbf{Q}, -\mathbf{Q} + \mathbf{G}, \omega) + \chi_{AA}^R(-\mathbf{Q}, -\mathbf{Q} - \mathbf{G}, \omega) \right]^\dagger.$$

We conclude that the real and imaginary parts of the \mathbf{G} -symmetrized combination $\chi_{AA}^R(\mathbf{Q}, \mathbf{Q} + \mathbf{G}, \omega) + \chi_{AA}^R(\mathbf{Q}, \mathbf{Q} - \mathbf{G}, \omega)$ are even and odd functions of \mathbf{Q} , respectively.

We now make use of these symmetry properties for the evaluation of Eq. (14). We enucleate two subsets of the \mathbf{G}_\perp vectors: g^+ including the \mathbf{G}_\perp vectors with both Miller indexes $l_y, l_z \geq 0$, and g^- including those with $l_y > 0$ and $l_z < 0$. To include the remaining $l_y < 0$ terms, we write:

$$\sum_{\mathbf{G}_\perp} \chi_{nn}^R(\mathbf{Q}, \mathbf{Q} + \mathbf{G}_\perp, \mathbf{Q} \cdot \mathbf{v}_{\text{SL}}) = \quad (\text{B6}) \\ = \sum_{\mathbf{G}_\perp \in g^+} \left[\chi_{nn}^R(\mathbf{Q}, \mathbf{Q} + \mathbf{G}_\perp, \mathbf{Q} \cdot \mathbf{v}_{\text{SL}}) \right. \\ \left. + \chi_{nn}^R(\mathbf{Q}, \mathbf{Q} - \mathbf{G}_\perp, \mathbf{Q} \cdot \mathbf{v}_{\text{SL}}) \right] + \\ + \sum_{\mathbf{G}_\perp \in g^-} \left[\chi_{nn}^R(\mathbf{Q}, \mathbf{Q} + \mathbf{G}_\perp, \mathbf{Q} \cdot \mathbf{v}_{\text{SL}}) \right. \\ \left. + \chi_{nn}^R(\mathbf{Q}, \mathbf{Q} - \mathbf{G}_\perp, \mathbf{Q} \cdot \mathbf{v}_{\text{SL}}) \right].$$

This summation does not include all \mathbf{G}_\perp -dependent factors in Eq. (14): we must restore the initial-condition

phase factor and the Fourier transform of the interaction potential. In fact, neither of these terms affects this symmetry property: the phase factor is independent of \mathbf{Q} , therefore it cannot change this symmetry; $\tilde{V}(|\mathbf{Q}|)$ is a real function. We conclude that:

$$\chi_{nn}^R(\mathbf{Q}, \mathbf{Q} + \mathbf{G}_\perp, \mathbf{Q} \cdot \mathbf{v}_{\text{SL}}) \tilde{V}(|\mathbf{Q} + \mathbf{G}_\perp|) + \quad (\text{B7}) \\ \chi_{nn}^R(\mathbf{Q}, \mathbf{Q} - \mathbf{G}_\perp, \mathbf{Q} \cdot \mathbf{v}_{\text{SL}}) \tilde{V}(|\mathbf{Q} - \mathbf{G}_\perp|) = \\ \left[\chi_{nn}^R(-\mathbf{Q}, -\mathbf{Q} + \mathbf{G}_\perp, -\mathbf{Q} \cdot \mathbf{v}_{\text{SL}}) \tilde{V}(|-\mathbf{Q} + \mathbf{G}_\perp|) + \right. \\ \left. \chi_{nn}^R(-\mathbf{Q}, -\mathbf{Q} - \mathbf{G}_\perp, -\mathbf{Q} \cdot \mathbf{v}_{\text{SL}}) \tilde{V}(|-\mathbf{Q} - \mathbf{G}_\perp|) \right]^*.$$

Appendix C: Retarded linear-response function

Here we derive expressions for the density-density response function, first for the standard conservative harmonic crystal, then for a crystal characterized by dissipative phonons.

1. Conservative crystal

We start from a regular conservative crystal. We express the retarded LR function

$$\chi_{nn}^R(\mathbf{x}, \mathbf{x}', t - t') \equiv -\frac{i}{\hbar} \theta(t - t') \langle [n(\mathbf{x}, t - t'), n(\mathbf{x}', 0)] \rangle \quad (\text{C1})$$

in its Fourier representation:

$$\chi_{nn}^R(\mathbf{Q}, \mathbf{Q} + \mathbf{G}_\perp, \omega) \quad (\text{C2}) \\ = \lim_{V \rightarrow \infty} -\frac{i}{\hbar} \int dt \theta(t) e^{i\omega t} \frac{1}{V} \int_V d^3x \int_V d^3x' \\ \times e^{-i\mathbf{Q}\cdot\mathbf{x}} e^{i(\mathbf{Q}+\mathbf{G}_\perp)\cdot\mathbf{x}'} \langle [n(\mathbf{x}, t), n(\mathbf{x}', 0)] \rangle \\ = \lim_{V \rightarrow \infty} -\frac{i}{\hbar V} \int dt \theta(t) e^{i\omega t} \\ \times \langle [n(\mathbf{Q}, t), n(-\mathbf{Q} - \mathbf{G}_\perp, 0)] \rangle.$$

Here we introduced

$$n(\mathbf{Q}, t) = \int_V d^3x e^{-i\mathbf{Q}\cdot\mathbf{x}} n(\mathbf{x}, t), \quad (\text{C3})$$

the spatial Fourier transform of the density operator. As customary for the vibrations of a crystal, we express the position operator of the j -th atom at time t as

$$\mathbf{x}_j = \mathbf{R}_j + \mathbf{u}_j(t), \quad (\text{C4})$$

the sum of its equilibrium position \mathbf{R}_j plus its displacement operator $\mathbf{u}_j(t)$. We substitute this decomposition into the definition (6) of the density operator, obtaining

$$n(\mathbf{Q}, t) = \int_V d^3x e^{-i\mathbf{Q}\cdot\mathbf{x}} \sum_{j=1}^N \delta^{(3)}(\mathbf{x} - \mathbf{x}_j) \quad (\text{C5}) \\ = \sum_{j=1}^N e^{-i\mathbf{Q}\cdot\mathbf{R}_j} e^{-i\mathbf{Q}\cdot\mathbf{u}_j(t)}.$$

N is the number of atoms in the crystal, hence the volume $V = Na^3$. Periodic boundary conditions are assumed to preserve crystalline symmetry. In 2D, Eq. (C5) the Dirac

deltas and the \mathbf{x} -integration become two-dimensional.

Equation (C2) involves the density-density correlation function in the Fourier domain:

$$\begin{aligned} \langle n(\mathbf{Q}, t) n(-\mathbf{Q} - \mathbf{G}_\perp, 0) \rangle &= \sum_{j, j'} e^{-i\mathbf{Q} \cdot (\mathbf{R}_j - \mathbf{R}_{j'})} \left\langle e^{-i\mathbf{u}_j(t) \cdot \mathbf{Q}} e^{i\mathbf{u}_{j'}(0) \cdot (\mathbf{Q} + \mathbf{G}_\perp)} \right\rangle \\ &= N \sum_j e^{-i\mathbf{Q} \cdot \mathbf{R}_j} \left\langle e^{-i\mathbf{u}_j(t) \cdot \mathbf{Q}} e^{i\mathbf{u}_0(0) \cdot (\mathbf{Q} + \mathbf{G}_\perp)} \right\rangle, \end{aligned} \quad (\text{C6})$$

where \mathbf{u}_0 is the displacement operator of an atom at an arbitrarily fixed site, say the origin $\mathbf{R}_0 = \mathbf{0}$. To evaluate these quantum averages, we use the Gaussian identity

$$\langle e^A e^B \rangle = e^{\frac{1}{2}\langle A^2 \rangle + \frac{1}{2}\langle B^2 \rangle + \langle AB \rangle} \quad (\text{C7})$$

valid for harmonic-oscillator operators.¹⁸ The direct application of Eq. (C7) to our case of interest, leads to:

$$\left\langle e^{-i\mathbf{u}_j(t) \cdot \mathbf{Q}} e^{i\mathbf{u}_0(0) \cdot (\mathbf{Q} + \mathbf{G}_\perp)} \right\rangle = e^{-\frac{1}{2}\langle \mathbf{u}_j(t) \cdot \mathbf{Q} \mathbf{u}_j(t) \cdot \mathbf{Q} \rangle} e^{-\frac{1}{2}\langle \mathbf{u}_0(0) \cdot (\mathbf{Q} + \mathbf{G}_\perp) \mathbf{u}_0(0) \cdot (\mathbf{Q} + \mathbf{G}_\perp) \rangle} e^{\langle \mathbf{u}_j(t) \cdot \mathbf{Q} \mathbf{u}_0(0) \cdot (\mathbf{Q} + \mathbf{G}_\perp) \rangle}. \quad (\text{C8})$$

To evaluate these averages, we express the displacement operators in terms of phonon annihilation $b_{\mathbf{k}\lambda}$ and creation $b_{\mathbf{k}\lambda}^\dagger$ operators¹⁹

$$\begin{aligned} \mathbf{u}_j(t) &= \frac{1}{\sqrt{N}} \sum_{\mathbf{k}, \lambda} \sqrt{\frac{\hbar}{2m\omega_\lambda(\mathbf{k})}} \epsilon_\lambda(\mathbf{k}) e^{i\mathbf{k} \cdot \mathbf{R}_j} \\ &\times \left(e^{-i\omega_\lambda(\mathbf{k})t} b_{\mathbf{k}\lambda} + e^{i\omega_\lambda(\mathbf{k})t} b_{-\mathbf{k}\lambda}^\dagger \right). \end{aligned} \quad (\text{C9})$$

We start calculating the equal-time quantum average

$$\begin{aligned} \langle \mathbf{u}_j(t) \cdot \mathbf{Q} \mathbf{u}_j(t) \cdot \mathbf{Q} \rangle &= \langle \mathbf{u}_0(0) \cdot \mathbf{Q} \mathbf{u}_0(0) \cdot \mathbf{Q} \rangle \\ &= \frac{1}{N} \sum_{\mathbf{k}, \mathbf{k}'} \sum_{\lambda, \lambda'} \mathbf{Q} \cdot \epsilon_\lambda(\mathbf{k}) \mathbf{Q} \cdot \epsilon_{\lambda'}(\mathbf{k}') \frac{\hbar}{2m\sqrt{\omega_\lambda(\mathbf{k})\omega_{\lambda'}(\mathbf{k}')}} \\ &\times \left\langle \left(e^{-i\omega_{\lambda'}(\mathbf{k}')t} b_{\mathbf{k}'\lambda'} + e^{i\omega_{\lambda'}(\mathbf{k}')t} b_{-\mathbf{k}'\lambda'}^\dagger \right) \right. \\ &\times \left. \left(e^{-i\omega_\lambda(\mathbf{k})t} b_{\mathbf{k}\lambda} + e^{i\omega_\lambda(\mathbf{k})t} b_{-\mathbf{k}\lambda}^\dagger \right) \right\rangle = \\ &= \frac{1}{N} \sum_{\mathbf{k}, \mathbf{k}'} \sum_{\lambda, \lambda'} \mathbf{Q} \cdot \epsilon_\lambda(\mathbf{k}) \mathbf{Q} \cdot \epsilon_{\lambda'}(\mathbf{k}') \frac{\hbar}{2m\sqrt{\omega_\lambda(\mathbf{k})\omega_{\lambda'}(\mathbf{k}')}} \\ &\times \left[e^{-i(\omega_\lambda(\mathbf{k}) - \omega_{\lambda'}(\mathbf{k}'))t} \left\langle b_{-\mathbf{k}'\lambda'}^\dagger b_{\mathbf{k}\lambda} \right\rangle \right. \\ &\left. + e^{i(\omega_\lambda(\mathbf{k}) - \omega_{\lambda'}(\mathbf{k}'))t} \left\langle b_{\mathbf{k}'\lambda'} b_{-\mathbf{k}\lambda}^\dagger \right\rangle \right], \end{aligned}$$

calculating the quantum average between creation and annihilation operators as

$$\begin{aligned} \left\langle b_{-\mathbf{k}'\lambda'}^\dagger b_{\mathbf{k}\lambda} \right\rangle &= \delta_{\mathbf{k}, -\mathbf{k}'} \delta_{\lambda, \lambda'} n_\lambda(\mathbf{k}) \\ \left\langle b_{\mathbf{k}'\lambda'} b_{-\mathbf{k}\lambda}^\dagger \right\rangle &= \delta_{\mathbf{k}, -\mathbf{k}'} \delta_{\lambda, \lambda'} (1 + n_\lambda(\mathbf{k})) \end{aligned} \quad (\text{C10})$$

and using the parity in \mathbf{k} of the phonon frequency (A10)

and of the polarization vectors we obtain

$$\begin{aligned} \langle \mathbf{u}_j(t) \cdot \mathbf{Q} \mathbf{u}_j(t) \cdot \mathbf{Q} \rangle &= \langle \mathbf{u}_0(0) \cdot \mathbf{Q} \mathbf{u}_0(0) \cdot \mathbf{Q} \rangle \\ &= \frac{1}{N} \sum_{\mathbf{k}, \lambda} |\mathbf{Q} \cdot \epsilon_\lambda(\mathbf{k})|^2 \frac{\hbar}{2m\omega_\lambda(\mathbf{k})} (2n_\lambda(\mathbf{k}) + 1) \\ &\equiv 2W(\mathbf{Q}), \end{aligned} \quad (\text{C11})$$

and, likewise,

$$\langle \mathbf{u}_0(0) \cdot (\mathbf{Q} + \mathbf{G}_\perp) \mathbf{u}_0(0) \cdot (\mathbf{Q} + \mathbf{G}_\perp) \rangle \equiv 2W(\mathbf{Q} + \mathbf{G}_\perp). \quad (\text{C12})$$

Here $n_\lambda(\mathbf{k}) = 1/(e^{\beta\hbar\omega_\lambda(\mathbf{k})} - 1)$ is the average number of quanta in the oscillator labeled by \mathbf{k} and λ at equilibrium at temperature $T = 1/(k_B\beta)$. Since all Bose excitation factors $n_\lambda(\mathbf{k})$ increase with temperature, so does the thermal vibration amplitude of the crystal, with the result that the value of these Debye-Waller¹⁹ factors $e^{-W(\mathbf{Q})}$ decreases. When the temperature becomes so high that $\beta\hbar\omega_\lambda(\mathbf{k}) \ll 1$ the crystal is packed with phonons, i.e. $n_\lambda(\mathbf{k}) \simeq k_B T / (\hbar\omega_\lambda(\mathbf{k})) \gg 1$, also $W(\mathbf{Q})$ is very large, and, as a result, the Debye-Waller factor decays rapidly toward zero. As a result, the friction force is also reduced: this ubiquitous effect, named thermolubricity, was studied in several different contexts.²⁰⁻²⁴ Note that the Debye-Waller factors are similar for the two terms generated by the commutator in Eq. (C2).

The third factor in Eq. (C8) is the only one that explicitly depends on time. Therefore both elements of the commutator in Eq. (C2) need to be calculated. We start

evaluating the first one

$$\begin{aligned}
& \langle \mathbf{u}_j(t) \cdot \mathbf{Q} \mathbf{u}_0(0) \cdot (\mathbf{Q} + \mathbf{G}_\perp) \rangle \quad (\text{C13}) \\
&= \frac{\hbar}{2mN} \sum_{\mathbf{k}, \mathbf{k}'} \sum_{\lambda, \lambda'} \frac{\mathbf{Q} \cdot \boldsymbol{\epsilon}_\lambda(\mathbf{k})(\mathbf{Q} + \mathbf{G}_\perp) \cdot \boldsymbol{\epsilon}_{\lambda'}(\mathbf{k}')}{\sqrt{\omega_\lambda(\mathbf{k})\omega_{\lambda'}(\mathbf{k}')}} e^{i\mathbf{k}' \cdot \mathbf{R}_j} \\
&\times \left\langle \left(e^{-i\omega_{\lambda'}(\mathbf{k}')t} b_{\mathbf{k}'\lambda'} + e^{i\omega_{\lambda'}(\mathbf{k}')t} b_{-\mathbf{k}'\lambda'}^\dagger \right) \left(b_{\mathbf{k}\lambda} + b_{-\mathbf{k}\lambda}^\dagger \right) \right\rangle \\
&= \frac{\hbar}{2mN} \sum_{\mathbf{k}, \mathbf{k}'} \sum_{\lambda, \lambda'} \frac{\mathbf{Q} \cdot \boldsymbol{\epsilon}_\lambda(\mathbf{k})(\mathbf{Q} + \mathbf{G}_\perp) \cdot \boldsymbol{\epsilon}_{\lambda'}(\mathbf{k}')}{\sqrt{\omega_\lambda(\mathbf{k})\omega_{\lambda'}(\mathbf{k}')}} e^{i\mathbf{k}' \cdot \mathbf{R}_j} \\
&\times \left[e^{i\omega_{\lambda'}(\mathbf{k}')t} \langle b_{-\mathbf{k}'\lambda'}^\dagger b_{\mathbf{k}\lambda} \rangle + e^{-i\omega_{\lambda'}(\mathbf{k}')t} \langle b_{\mathbf{k}'\lambda'} b_{-\mathbf{k}\lambda}^\dagger \rangle \right].
\end{aligned}$$

By evaluating the quantum average as in Eq. (C10) and using the parity in \mathbf{k} of the phonon frequency and of the polarization vector, as analyzed in Appendix A, we obtain

$$\begin{aligned}
& \langle \mathbf{u}_j(t) \cdot \mathbf{Q} \mathbf{u}_0(0) \cdot (\mathbf{Q} + \mathbf{G}_\perp) \rangle \quad (\text{C14}) \\
&= \frac{\hbar}{2mN} \sum_{\mathbf{k}} \sum_{\lambda} \frac{\mathbf{Q} \cdot \boldsymbol{\epsilon}_\lambda(\mathbf{k})(\mathbf{Q} + \mathbf{G}_\perp) \cdot \boldsymbol{\epsilon}_\lambda(\mathbf{k})}{\omega_\lambda(\mathbf{k})} \\
&\times e^{-i\mathbf{k} \cdot \mathbf{R}_j} \left[e^{i\omega_\lambda(\mathbf{k})t} n_\lambda(\mathbf{k}) + e^{-i\omega_\lambda(\mathbf{k})t} (1 + n_\lambda(\mathbf{k})) \right] \\
&= \frac{\hbar}{2mN} \sum_{\mathbf{k}} \sum_{\lambda} \frac{\mathbf{Q} \cdot \boldsymbol{\epsilon}_\lambda(\mathbf{k})(\mathbf{Q} + \mathbf{G}_\perp) \cdot \boldsymbol{\epsilon}_\lambda(\mathbf{k})}{\omega_\lambda(\mathbf{k})} e^{-i\mathbf{k} \cdot \mathbf{R}_j} \\
&\times [(2n_\lambda(\mathbf{k}) + 1) \cos(\omega_\lambda(\mathbf{k})t) - i \sin(\omega_\lambda(\mathbf{k})t)].
\end{aligned}$$

Note that, for a crystal lattice with different symmetries, not all simplifications carried out in Eq. (C14) may apply.

Consider the other term $\langle \mathbf{u}_0(0) \cdot (\mathbf{Q} + \mathbf{G}_\perp) \mathbf{u}_j(t) \cdot \mathbf{Q} \rangle$, arising in the calculation of the commutator in Eq. (C2), processed through Eq. (C8). With a similar derivation, we obtain an expression which is the complex conjugate of the result of Eq. (C14):

$$\begin{aligned}
& \langle \mathbf{u}_0(0) \cdot (\mathbf{Q} + \mathbf{G}_\perp) \mathbf{u}_j(t) \cdot \mathbf{Q} \rangle \quad (\text{C15}) \\
&= \frac{\hbar}{2mN} \sum_{\mathbf{k}} \sum_{\lambda} \frac{\mathbf{Q} \cdot \boldsymbol{\epsilon}_\lambda(\mathbf{k})(\mathbf{Q} + \mathbf{G}_\perp) \cdot \boldsymbol{\epsilon}_\lambda(\mathbf{k})}{\omega_\lambda(\mathbf{k})} e^{-i\mathbf{k} \cdot \mathbf{R}_j} \\
&\times [(2n_\lambda(\mathbf{k}) + 1) \cos(\omega_\lambda(\mathbf{k})t) + i \sin(\omega_\lambda(\mathbf{k})t)].
\end{aligned}$$

At this point, it is convenient to define

$$\begin{aligned}
\phi_j(t, \beta) &\equiv \langle \mathbf{u}_j(t) \cdot \mathbf{Q} \mathbf{u}_0(0) \cdot (\mathbf{Q} + \mathbf{G}_\perp) \rangle \quad (\text{C16}) \\
&= \langle \mathbf{u}_0(0) \cdot (\mathbf{Q} + \mathbf{G}_\perp) \mathbf{u}_j(t) \cdot \mathbf{Q} \rangle^\dagger.
\end{aligned}$$

Observe that the real part of $\phi_j(t, \beta)$ depends both on time and on temperature, while its imaginary part is independent of temperature:

$$\begin{aligned}
\phi_j(t, \beta) &= \text{Re} \phi_j(t, \beta) + i \text{Im} \phi_j(t, \beta) \quad (\text{C17}) \\
&= \phi_j^r(t, \beta) + i \phi_j^i(t).
\end{aligned}$$

This same observation applies also for the 1D counterpart of this formula.⁶

We have now all elements required to write an explicit expression for the Fourier representation of the relevant

density-density response function, Eq. (C2):

$$\begin{aligned}
\chi_{nn}^R(\mathbf{Q}, \mathbf{Q} + \mathbf{G}_\perp, \omega) &= -\frac{i}{\hbar a^3} e^{-W(\mathbf{Q})} e^{-W(\mathbf{Q} + \mathbf{G}_\perp)} \quad (\text{C18}) \\
&\times \int dt \theta(t) e^{i\omega t} \sum_{j=0}^{N-1} e^{-i\mathbf{Q} \cdot \mathbf{R}_j} \left[e^{\phi_j(t, \beta)} - e^{\phi_j^\dagger(t, \beta)} \right] \\
&= -\frac{i}{\hbar a^3} e^{-W(\mathbf{Q})} e^{-W(\mathbf{Q} + \mathbf{G}_\perp)} \\
&\times \int dt \theta(t) e^{i\omega t} \sum_{j=0}^{N-1} e^{-i\mathbf{Q} \cdot \mathbf{R}_j} e^{\phi_j^r(t, \beta)} \\
&\times \left[e^{i\phi_j^i(t)} - e^{-i\phi_j^i(t)} \right] \\
&= \frac{2}{\hbar a^3} e^{-W(\mathbf{Q})} e^{-W(\mathbf{Q} + \mathbf{G}_\perp)} \int dt \theta(t) e^{i\omega t} \\
&\times \sum_{j=0}^{N-1} e^{-i\mathbf{Q} \cdot \mathbf{R}_j} e^{\phi_j^r(t, \beta)} \sin(\phi_j^i(t)).
\end{aligned}$$

This is an exact expression for the retarded density-density LR function of the vibrating harmonic lattice. Evaluating $\chi_{nn}^R(\mathbf{Q}, \mathbf{Q} + \mathbf{G}_\perp, \omega)$ through Eq. (C18) requires carrying out a double integration, namely over the \mathbf{k} points in the BZ (in $\phi_j(t, \beta)$) and over time, plus a summation over the lattice translations, which makes it quite cumbersome and inefficient to compute numerically. Unfortunately, we cannot see a way to further simplify the final expression Eq. (C18), while keeping it exact.

As was done for the 1D problem,⁶ we resort to the one-phonon approximation¹⁹ for the terms involving $\phi_j(t, \beta)$:

$$e^{\phi_j^r(t, \beta)} \sin(\phi_j^i(t)) \simeq \phi_j^i(t), \quad (\text{C19})$$

which is valid in the limit of small $|\phi_j(t, \beta)|$, appropriate for not too large wave vector Q and not too high temperature. By inserting the one-phonon approximation (C19) in Eq. (C18), we obtain

$$\begin{aligned}
\chi_{nn}^{R1 \text{ Ph}}(\mathbf{Q}, \mathbf{Q} + \mathbf{G}_\perp, \omega) &\quad (\text{C20}) \\
&\simeq \frac{2}{\hbar a^3} e^{-W(\mathbf{Q})} e^{-W(\mathbf{Q} + \mathbf{G}_\perp)} \int dt \theta(t) e^{i\omega t} \sum_{j=0}^{N-1} e^{-i\mathbf{Q} \cdot \mathbf{R}_j} \\
&\times \frac{(-\hbar)}{2mN} \sum_{\mathbf{k}, \lambda} \frac{\mathbf{Q} \cdot \boldsymbol{\epsilon}_\lambda(\mathbf{k})(\mathbf{Q} + \mathbf{G}_\perp) \cdot \boldsymbol{\epsilon}_\lambda(\mathbf{k})}{\omega_\lambda(\mathbf{k})} \\
&\times e^{-i\mathbf{k} \cdot \mathbf{R}_j} \sin(\omega_\lambda(\mathbf{k})t) \\
&= -\frac{1}{m a^3 N} e^{-W(\mathbf{Q})} e^{-W(\mathbf{Q} + \mathbf{G}_\perp)} \int dt \theta(t) e^{i\omega t} \\
&\times \sum_{j=0}^{N-1} e^{-i\mathbf{Q} \cdot \mathbf{R}_j} \sum_{\mathbf{k}, \lambda} \frac{\mathbf{Q} \cdot \boldsymbol{\epsilon}_\lambda(\mathbf{k})(\mathbf{Q} + \mathbf{G}_\perp) \cdot \boldsymbol{\epsilon}_\lambda(\mathbf{k})}{\omega_\lambda(\mathbf{k})} \\
&\times e^{-i\mathbf{k} \cdot \mathbf{R}_j} \sin(\omega_\lambda(\mathbf{k})t).
\end{aligned}$$

Here, the simplification of Planck's constant indicates that in the one-phonon approximation the only quantum

effects occur through the Debye-Waller factors. Executing the thermodynamic limit we obtain:

$$\begin{aligned} \chi_{nn}^{R1 \text{ ph}}(\mathbf{Q}, \mathbf{Q} + \mathbf{G}_\perp, \omega) & \quad (\text{C21}) \\ &= -\frac{1}{m} e^{-W(\mathbf{Q})} e^{-W(\mathbf{Q} + \mathbf{G}_\perp)} \int dt \theta(t) e^{i\omega t} \sum_j e^{-i\mathbf{Q} \cdot \mathbf{R}_j} \\ & \times \sum_\lambda \int_{BZ} \frac{d^3 k}{(2\pi)^3} \frac{\mathbf{Q} \cdot \boldsymbol{\epsilon}_\lambda(\mathbf{k}) (\mathbf{Q} + \mathbf{G}_\perp) \cdot \boldsymbol{\epsilon}_\lambda(\mathbf{k})}{\omega_\lambda(\mathbf{k})} \\ & \times e^{-i\mathbf{k} \cdot \mathbf{R}_j} \sin(\omega_\lambda(\mathbf{k})t), \end{aligned}$$

where the integral over \mathbf{k} extends over the first Brillouin zone, and the sum over j spans the infinitely-many translations \mathbf{R}_j of the Bravais lattice. To simplify this expression we can use the identity $\sin(x) = (e^{ix} - e^{-ix})/(2i)$. Accordingly,

$$\begin{aligned} \chi_{nn}^{R1 \text{ ph}}(\mathbf{Q}, \mathbf{Q} + \mathbf{G}_\perp, \omega) & \quad (\text{C22}) \\ &= \frac{i}{2m} e^{-W(\mathbf{Q})} e^{-W(\mathbf{Q} + \mathbf{G}_\perp)} \int dt \theta(t) \\ & \times \sum_j \sum_\lambda \int_{BZ} \frac{d^3 k}{(2\pi)^3} e^{-i\mathbf{R}_j \cdot (\mathbf{Q} - \mathbf{k})} \\ & \times \frac{\mathbf{Q} \cdot \boldsymbol{\epsilon}_\lambda(\mathbf{k}) (\mathbf{Q} + \mathbf{G}_\perp) \cdot \boldsymbol{\epsilon}_\lambda(\mathbf{k})}{\omega_\lambda(\mathbf{k})} \\ & \times \left[e^{it(\omega_\lambda(\mathbf{k}) + \omega)} - e^{-it(\omega_\lambda(\mathbf{k}) - \omega)} \right]. \end{aligned}$$

Now we make use of the 3D version of the periodic delta function, or *Dirac comb*, identity:

$$\sum_j e^{-i\mathbf{R}_j \cdot (\mathbf{Q} - \mathbf{k})} = \frac{(2\pi)^3}{a^3} \sum_{\mathbf{G}'} \delta^3(\mathbf{k} - \mathbf{Q} - \mathbf{G}'), \quad (\text{C23})$$

where $\mathbf{G}' = \frac{2\pi}{a}(l_x, l_y, l_z)$ are the reciprocal lattice vectors of the Bravais lattice. Hence, combining the integral over \mathbf{k} extended over the first BZ with the \mathbf{G}' summation, we obtain an unrestricted integral on a variable $\mathbf{k}' = \mathbf{k} - \mathbf{G}'$ spanning the the entire reciprocal space. Furthermore, the $\delta^3(\mathbf{k}' - \mathbf{Q})$ condition eliminates the integration over \mathbf{k}' , and fixes \mathbf{k}' to \mathbf{Q} . We rewrite Eq. (C22) as

$$\begin{aligned} \chi_{nn}^{R1 \text{ ph}}(\mathbf{Q}, \mathbf{Q} + \mathbf{G}_\perp, \omega) & \quad (\text{C24}) \\ &= \frac{i}{2ma^3} e^{-W(\mathbf{Q})} e^{-W(\mathbf{Q} + \mathbf{G}_\perp)} \\ & \times \sum_\lambda \frac{\mathbf{Q} \cdot \boldsymbol{\epsilon}_\lambda(\mathbf{Q}) (\mathbf{Q} + \mathbf{G}_\perp) \cdot \boldsymbol{\epsilon}_\lambda(\mathbf{Q})}{\omega_\lambda(\mathbf{Q})} \\ & \times \int dt \theta(t) \left[e^{it(\omega + \omega_\lambda(\mathbf{Q}))} - e^{it(\omega - \omega_\lambda(\mathbf{Q}))} \right]. \end{aligned}$$

Since all factors in Eq. (C24) except for the initial imaginary unit and the final time integral are real, and we are interested in the imaginary part of χ_{nn}^R only, we need to evaluate the real part of the time integral only. We recall the real part of the Fourier transform of the Heaviside θ function:

$$\text{Re} \int dt \theta(t) e^{i\omega t} = \pi \delta(\omega). \quad (\text{C25})$$

Accordingly,

$$\begin{aligned} \text{Im} \chi_{nn}^{R1 \text{ ph}}(\mathbf{Q}, \mathbf{Q} + \mathbf{G}_\perp, \omega) & \quad (\text{C26}) \\ &= \frac{\pi}{2ma^3} e^{-W(\mathbf{Q})} e^{-W(\mathbf{Q} + \mathbf{G}_\perp)} \\ & \times \sum_\lambda \frac{\mathbf{Q} \cdot \boldsymbol{\epsilon}_\lambda(\mathbf{Q}) (\mathbf{Q} + \mathbf{G}_\perp) \cdot \boldsymbol{\epsilon}_\lambda(\mathbf{Q})}{\omega_\lambda(\mathbf{Q})} \\ & \times [\delta(\omega + \omega_\lambda(\mathbf{Q})) - \delta(\omega - \omega_\lambda(\mathbf{Q}))]. \end{aligned}$$

In Sect. IV A, we adopt this approximate expression for the calculation of friction.

2. Dissipative crystal

The next step is the introduction of a finite phonon lifetime. For this purpose, we add a small imaginary part to the frequency: $\omega \rightarrow \omega + i\gamma/2$. This modification introduces a uniform exponential decay with rate $\gamma/2$ to all phonon modes, corresponding to a lifetime $2/\gamma$. With this phenomenological modification, we rewrite the retarded one-phonon-approximate LR function, Eq. (C24), as follows:

$$\begin{aligned} \chi_{nn}^{R1 \text{ ph}}(\mathbf{Q}, \mathbf{Q} + \mathbf{G}_\perp, \omega) & \quad (\text{C27}) \\ &= \frac{i}{2ma^3} e^{-W(\mathbf{Q})} e^{-W(\mathbf{Q} + \mathbf{G}_\perp)} \\ & \times \sum_\lambda \frac{\mathbf{Q} \cdot \boldsymbol{\epsilon}_\lambda(\mathbf{Q}) (\mathbf{Q} + \mathbf{G}_\perp) \cdot \boldsymbol{\epsilon}_\lambda(\mathbf{Q})}{\omega_\lambda(\mathbf{Q})} \\ & \times \int dt \theta(t) (e^{it(\omega + \omega_\lambda(\mathbf{Q}) + i\frac{\gamma}{2})} - e^{it(\omega - \omega_\lambda(\mathbf{Q}) + i\frac{\gamma}{2})}). \end{aligned}$$

The time integration is of this elementary form:

$$\int_{-\infty}^{+\infty} dt \theta(t) e^{it(\omega + i\frac{\gamma}{2})} = \int_0^{+\infty} dt e^{it(\omega + i\frac{\gamma}{2})} = \frac{i}{\omega + i\frac{\gamma}{2}}. \quad (\text{C28})$$

Therefore, the time integral in the last line of Eq. (C27) becomes:

$$\begin{aligned} & \int_{-\infty}^{+\infty} dt \theta(t) \left(e^{it(\omega + \omega_\lambda(\mathbf{Q}) + i\frac{\gamma}{2})} - e^{it(\omega - \omega_\lambda(\mathbf{Q}) + i\frac{\gamma}{2})} \right) \\ &= i \left(\frac{1}{\omega + \omega_\lambda(\mathbf{Q}) + i\frac{\gamma}{2}} - \frac{1}{\omega - \omega_\lambda(\mathbf{Q}) + i\frac{\gamma}{2}} \right) \quad (\text{C29}) \\ &= i \left(\frac{\omega + \omega_\lambda(\mathbf{Q}) - i\frac{\gamma}{2}}{(\omega + \omega_\lambda(\mathbf{Q}))^2 + (\frac{\gamma}{2})^2} - \frac{\omega - \omega_\lambda(\mathbf{Q}) - i\frac{\gamma}{2}}{(\omega - \omega_\lambda(\mathbf{Q}))^2 + (\frac{\gamma}{2})^2} \right) \\ &= \left(\frac{i(\omega + \omega_\lambda(\mathbf{Q})) + \frac{\gamma}{2}}{(\omega + \omega_\lambda(\mathbf{Q}))^2 + (\frac{\gamma}{2})^2} - \frac{i(\omega - \omega_\lambda(\mathbf{Q})) + \frac{\gamma}{2}}{(\omega - \omega_\lambda(\mathbf{Q}))^2 + (\frac{\gamma}{2})^2} \right). \end{aligned}$$

In the last expressions we have separated the real and imaginary parts of both fractions. All other factors in Eq. (C27) being real except for the initial imaginary unit, the imaginary part of $\chi_{nn}^{R1 \text{ ph}}$ is obtained by retaining the

real part of the result of the time integration in Eq. (C29):

$$\begin{aligned} \text{Im } \chi_{nn}^{R1 \text{ ph}}(\mathbf{Q}, \mathbf{Q} + \mathbf{G}_\perp, \omega) & \quad (\text{C30}) \\ &= \frac{\pi}{2ma^3} e^{-W(\mathbf{Q})} e^{-W(\mathbf{Q} + \mathbf{G}_\perp)} \\ &\times \sum_\lambda \frac{\mathbf{Q} \cdot \boldsymbol{\epsilon}_\lambda(\mathbf{Q}) (\mathbf{Q} + \mathbf{G}_\perp) \cdot \boldsymbol{\epsilon}_\lambda(\mathbf{Q})}{\omega_\lambda(\mathbf{Q})} \\ &\times \left[\frac{\frac{\gamma}{2\pi}}{(\omega + \omega_\lambda(\mathbf{Q}))^2 + (\frac{\gamma}{2})^2} - \frac{\frac{\gamma}{2\pi}}{(\omega - \omega_\lambda(\mathbf{Q}))^2 + (\frac{\gamma}{2})^2} \right]. \end{aligned}$$

A comparison of Eq. (C30) with the infinite-lifetime expression (C26) shows that the introduction of dissipation has the unique effect of broadening the Dirac $\delta(\omega - \omega_\lambda(\mathbf{Q}))$ to a Lorentzian:

$$\delta(\omega_\lambda(\mathbf{Q}) - \omega) \rightarrow \frac{\frac{\gamma}{2\pi}}{(\omega - \omega_\lambda(\mathbf{Q}))^2 + (\frac{\gamma}{2})^2}. \quad (\text{C31})$$

In Sect. IV B, we adopt the one-phonon expression (C30) for the evaluation of friction in the dissipative crystal.

Appendix D: Molecular-dynamics simulations

We simulate a cubic portion of the harmonic simple-cubic lattice consisting of $N = 51 \times 51 \times 51$ atoms. For the 2D model, we consider a square portion of the harmonic square lattice involving $N = 201 \times 201$ atoms. In both models, atoms are connected by nearest-neighbor springs (with strength K and rest length a), and second-neighbor springs (with strength $K' = K/2$ and rest length $\sqrt{2}a$). We apply periodic boundary conditions to mitigate finite-size effects.

We integrate $T = 0$ Langevin equations of motion, with a viscous term with damping coefficient γ , adopting the values discussed in Sects. V and VI. Numerical integration relies on an accurate Runge-Kutta-Feldberg algorithm that adapts its time step to maintain a predetermined accuracy. The slider is kept advancing at the fixed speed v_{SL} along a line halfway between the rest positions of two adjacent atomic rows or through the center of a sequence of aligned cubes in the (100) direction. The slider and the crystal interact through the potential of Eq. (7), with the weak coupling amplitude $\varepsilon = 5 \times 10^{-4} K a^2$. In the simulations, we adopt a smoothly truncated version of $V(r)$, which vanishes beyond a cutoff distance $5a$. We typically run simulations over a total time as large as $2 \times 10^4 (m/K)^{1/2}$ for the lowest simulated speed $v_{\text{SL}} = 0.01 a(K/m)^{1/2}$, then progressively reduced to $1 \times 10^3 (m/K)^{1/2}$ for $v_{\text{SL}} \geq 0.2 a(K/m)^{1/2}$, in such a way that the slider advances by at least 200 lattice spacings in each simulation.

As the crystal starts off in its static equilibrium configuration, it needs some time to adjust itself to the presence of the advancing slider. We consider the simulation steps covering the initial $150 (m/K)^{1/2}$ time interval as a transient, and therefore we omit them from the evaluation of steady-state average properties. By monitoring

the average kinetic energy of the crystal lattice, we verified that the crystal average temperature never exceeds a tiny $T = 4 \times 10^{-10} K a^2/k_B$, indicating that simulations are indeed representative of the $T = 0$ regime.

To compute the average friction force, in principle one could evaluate the time average of the force experienced by the slider. However, this procedure is numerically quite challenging, since the slider force in the advancing direction oscillates widely, with instantaneous values of the order of ε/σ . This fluctuation is several orders of magnitude larger than its sought-for average value which, according to Eq. (33), is very small, of order ε^2 . Therefore we rather evaluate F by means of a numerically more stable and convenient procedure: The advancing slider pushes the whole crystal forward by transferring to it a rightward momentum $\mathbf{F}(t)dt$. As a result, in the initial transient the center of mass of the crystal accelerates, but it soon acquires a nearly steady velocity \mathbf{V}_{CM} when the viscous force $-m\gamma\mathbf{v}_j$ that the Langevin thermostat applies to each crystal atom generates a total compensating leftward momentum transfer $\mathbf{F}_{\text{diss}}(t)dt = -m\gamma \sum_j \mathbf{v}_j dt$. This compensation is not exact at each instant of time: as a result, the crystal center of mass advances to the right at a not-exactly-constant velocity. However, in the steady state the fluctuations of $\mathbf{V}_{\text{CM}} = N^{-1} \sum_j \mathbf{v}_j$ are a tiny fraction of its average value, due to the huge inertia of the crystal ($N \gg 1$). Moreover, for the adopted small coupling ε , the value of $|\mathbf{V}_{\text{CM}}|$ is quite small, never exceeding $1.6 \times 10^{-9} a(K/m)^{1/2}$. In practice, the time-average of \mathbf{V}_{CM} is obtained by the numerically extremely stable and reliable expression

$$\bar{\mathbf{V}}_{\text{CM}} \equiv \frac{1}{t_2 - t_1} \int_{t_1}^{t_2} \mathbf{V}_{\text{CM}}(t) dt = \frac{\mathbf{X}_{\text{CM}}(t_2) - \mathbf{X}_{\text{CM}}(t_1)}{t_2 - t_1}, \quad (\text{D1})$$

evaluated with t_1 at the end of the initial transient and t_2 at the end of the simulation. Given $\bar{\mathbf{V}}_{\text{CM}}$ from a simulation, then the average friction force is evaluated as

$$\mathbf{F} = Nm\gamma \bar{\mathbf{V}}_{\text{CM}}. \quad (\text{D2})$$

Of course, in all these vectors, the transverse components vanish: only the component in the $\hat{\mathbf{e}}_x$ sliding direction is relevant. For example, $F = F_x$ is the quantity reported as circles in Figs. 4, 5, 9, and 11.

Appendix E: 3D Fourier Transform of the potential

In 3D, the FT is defined and evaluated as follows:

$$\begin{aligned} \tilde{V}(\mathbf{q}) &= \int d^3x e^{-i\mathbf{q}\cdot\mathbf{x}} V(|\mathbf{x}|) \\ &= 2\pi \int_0^{+\infty} dr r^2 V(r) \int_{-1}^{+1} d \cos \theta e^{-iqr \cos \theta} = \\ &= \frac{4\pi}{q} \int_0^{+\infty} dr r V(r) \sin(qr) \\ &= \tilde{V}(|\mathbf{q}|) = \tilde{V}(q). \end{aligned} \quad (\text{E1})$$

As noted in the final line, this sort of “atomic form factor of the slider” is a real function, and it is spherically symmetric in reciprocal space, i.e. \tilde{V} only depends on the length of the \mathbf{q} vector.

For evaluating this integral, we first proceed to manipulate

$$\tilde{V}(q) = \frac{4\pi}{q} \int_0^{+\infty} dr r V(r) \sin(qr), \quad (\text{E2})$$

using the relation $\sin(qr) = \frac{e^{iqr} - e^{-iqr}}{2i}$. Observe that the potential is even in r , which allows us to rewrite the integral as

$$\int_0^{+\infty} dr r V(r) \frac{e^{iqr} - e^{-iqr}}{2i} = \int_{-\infty}^{+\infty} dr r V(r) \frac{e^{iqr}}{2i}. \quad (\text{E3})$$

For our regularized LJ function, Eq. (7):

$$\begin{aligned} \tilde{V}(\mathbf{q}) &= \frac{4\pi\varepsilon}{q} \int_{-\infty}^{+\infty} dr r \\ &\left[\left(\frac{\sigma^2 + d^2}{r^2 + d^2} \right)^6 - 2 \left(\frac{\sigma^2 + d^2}{r^2 + d^2} \right)^3 \right] \frac{e^{iqr}}{2i}. \end{aligned} \quad (\text{E4})$$

To evaluate this integral, we consider the two terms in the sum separately. We start solving the simpler one

$$\int_{-\infty}^{+\infty} dr r \left(\frac{1}{r^2 + d^2} \right)^3 e^{iqr} \quad (\text{E5})$$

where all the constants are omitted. This function has triple poles at $r = \pm id$. Notice that due to the presence of e^{iqr} we close the integration in the upper half of the complex r plane. We recall the general expression for a residue of order n at location c :

$$\text{Res}(f(z), c) = \frac{1}{(n-1)!} \lim_{z \rightarrow c} \frac{d^{n-1}}{dz^{n-1}} [(z-c)^n f(z)]. \quad (\text{E6})$$

For our function and order 3:

$$\begin{aligned} \text{Res}(f(z), id) &= \frac{1}{2} \lim_{z \rightarrow id} \frac{d^2}{dz^2} \\ &\left[(z-id)^3 z \left(\frac{1}{(z+id)(z-id)} \right)^3 e^{iqz} \right] \\ &= \frac{1}{2} \lim_{z \rightarrow id} \frac{d^2}{dz^2} \left(z \frac{1}{(z+id)^3} e^{iqz} \right) \\ &= \frac{q}{16d^3} e^{-qd} (1+qd) \end{aligned} \quad (\text{E7})$$

using the residue theorem, this part gives the term with $(qd+1)$ in Eq. (8). With the same approach we calculate the remaining part, involving the integral

$$\int_{-\infty}^{+\infty} dr r \left(\frac{1}{r^2 + d^2} \right)^6 e^{iqr}. \quad (\text{E8})$$

The 6th order residue of this integrand is

$$\begin{aligned} \text{Res}(f(z), id) &= \frac{1}{5!} \lim_{z \rightarrow id} \frac{d^5}{dz^5} \left(z \frac{1}{(z+id)^6} e^{iqz} \right) \\ &= \frac{q e^{-qd}}{5! 2^6 d^9} [105 + 105qd + 45q^2 d^2 + 10q^3 d^3 + q^4 d^4] \end{aligned} \quad (\text{E9})$$

that generates the remaining terms in Eq. (8).

Appendix F: 2D Fourier Transform of the potential

The 2D Fourier transform of the interaction potential of Eq. (7) is:

$$\begin{aligned} \tilde{V}(q) &= \int d^2x e^{-i\mathbf{q}\cdot\mathbf{x}} V(|\mathbf{x}|) \\ &= \int_0^{+\infty} dr r V(r) \int_0^{2\pi} d\theta e^{-iqr \cos \theta} \\ &= 2\pi \int_0^{+\infty} dr r J_0(qr) V(r), \end{aligned} \quad (\text{F1})$$

where $J_0(\cdot)$ is the 0th-order Bessel function of the first kind.

To derive an explicit expression for the integral in Eq. (F1), we resort to Equation 10.22.46 of Ref. 25, that we specialize to $\nu = 0$ and reformulate as follows:

$$\int_0^{\infty} dr r J_0(qr) \frac{b^{2(n+1)}}{(r^2 + b^2)^{n+1}} = \frac{b^2}{n!} \left(\frac{qb}{2} \right)^n K_n(qb), \quad (\text{F2})$$

where $K_n(\cdot)$ is a modified Bessel function of the second kind. By applying this formula twice, namely with $n = 5$ and $n = 2$, we obtain the expression reported as Eq. (9).

Note that the divergences of the modified Bessel function of the second kind $K_n(qd)$ for $qd \rightarrow 0$ are compensated by the corresponding power terms, so that the $qd \rightarrow 0$ limit of Eq. (9) is finite, namely:

$$\tilde{V}(0) = 2\pi\varepsilon d^2 \left[\frac{1}{10} \left(1 + \frac{\sigma^2}{d^2} \right)^6 - \frac{1}{2} \left(1 + \frac{\sigma^2}{d^2} \right)^3 \right]. \quad (\text{F3})$$

In practice, the straightforward implementation of Eq. (9) based on the python `scipy.special` standard package is numerically stable down to $qd \geq 2 \times 10^{-9}$. Below this value of qd , our implementation returns the result of Eq. (F3).

-
- ¹ A. Einstein, *Ann. Phys.* **322**, 549 (1905).
- ² H. Callen and T. Welton, *Phys. Rev.* **83**, 34 (1951).
- ³ R. Kubo, *Rep. Prog. Phys.* **29**, 255 (1966).
- ⁴ L. Landau and E. Lifshitz, *Electrodynamics of Continuous Media* (Pergamon, Oxford, 1984).
- ⁵ D. Pines, *Elementary excitations in solids* (Perseus, Reading, 1999).
- ⁶ E. Panizon, G. E. Santoro, E. Tosatti, G. Riva, and N. Manini, *Phys. Rev. B* **97**, 104104 (2018).
- ⁷ E. Panizon, G.E. Santoro, E. Tosatti, G. Riva, and N. Manini, in print in *Phys. Rev. B* (2024).
- ⁸ R. Guerra, U. Tartaglino, A. Vanossi, and E. Tosatti, *Nat. Mater.* **9**, 634 (2010).
- ⁹ D. Gemmell, *Rev. Mod. Phys.* **46**, 129 (1974).
- ¹⁰ G. F. Giuliani and G. Vignale, *Quantum Theory of the Electron Liquid* (Cambridge Univ. Press, 2005).
- ¹¹ L. van Hove, *Phys. Rev.* **89**, 1189 (1953).
- ¹² S. V. Kozhevnikov, Y. N. Khaidukov, F. Ott, and F. Radu, *J. Exp. Theor. Phys.* **126**, 592 (2018).
- ¹³ V. G. Baryshevskii and A. M. Zaitseva, *phys. stat. sol. b* **157**, 129 (1990).
- ¹⁴ K. Korotchenko and Y. P. Kunashenko, *Nuovo Cimento* **34**, 537 (2011).
- ¹⁵ M. Bée, *Quasielastic Neutron Scattering* (Hilger, Bristol, 1988).
- ¹⁶ M. Lee, R. L. C. Vink, C. A. Volkert, and M. Krüger, *Phys. Rev. B* **104**, 174309 (2021).
- ¹⁷ A. Kamenev, *Field Theory of Non-Equilibrium Systems* (Cambridge Univ. Press, Cambridge, 2011).
- ¹⁸ N. Mermin, *J. Math. Phys.* **7**, 1038 (1966).
- ¹⁹ N. Ashcroft and M. Mermin, *Solid State Physics* (Holt-Saunders, Philadelphia, 1976).
- ²⁰ Y. Sang, M. Dubé, and M. Grant, *Phys. Rev. Lett.* **87**, 174301 (2001).
- ²¹ O. M. Dudko, A. Filippov, J. Klafter, and M. Urbakh, *Chem. Phys. Lett.* **352**, 499 (2002).
- ²² I. Szlufarska, M. Chandross, and R. Carpick, *J. Phys. D* **41**, 123001 (2008).
- ²³ M. Brukman, G. Gao, R. Nemanich, and J. Harrison, *J. Phys. Chem. C* **112**, 9358 (2008).
- ²⁴ P. Steiner, R. Roth, E. Gnecco, A. Baratoff, S. Maier, T. Glatzel, and E. Meyer, *Phys. Rev. B* **79**, 045414 (2009).
- ²⁵ F. W. J. Olver, A. B. O. Daalhuis, D. W. Lozier, B. I. Schneider, R. F. Boisvert, C. W. Clark, B. R. Miller, B. V. Saunders, H. S. Cohl, and M. A. McClain, eds., *NIST Digital Library of Mathematical Functions* (Release 1.1.11, 2023), URL <https://dlmf.nist.gov/10.22>.
- ²⁶ L. R. Logan, C. S. Murthy, and G. R. Srinivasan, *Phys. Rev. A* **46**, 5754 (1992).
- ²⁷ W. Scandale, M. D’Andrea, L. Esposito, M. Garattini, E. Guillermain, D. Mirarchi, S. Montesano, A. Natchii, R. Rossi, G. I. Smirnov, et al., *J. Inst.* **16**, P08015 (2021).
- ²⁸ Commonly channeled charged particles^{4,9,26,27} dissipate more energy through the excitation of electrons than through the generation of phonons that is addressed by the present theory.